 Bull. Chem. Soc. Jpn. Vol. 82, No. 6, 631–663 (2009)

Award Accounts

The Chemical Society of Japan Award for Creative Work for 2006

Phthalocyanine, Porphyrin, Cyclodextrin, and Polymer Systems Suitable for Studying by Circular Dichroism, Magnetic Circular Dichroism, and/or Electrochemistry

Nagao Kobayashi* and Takamitsu Fukuda

Department of Chemistry, Graduate School of Science, Tohoku University, Sendai 980-8578

Received May 20, 2008; E-mail: nagaok@mail.tains.tohoku.ac.jp

We introduce some representative studies from our laboratory, mostly from the 21st Century. We are interested in the synthesis, optical spectroscopy, such as magnetic circular dichroism (MCD), circular dichroism (CD), and electrochemistry of large aromatic molecules such as porphyrins and phthalocyanines, as well as cyclodextrin and polymer systems showing CD activity.

In this paper, we mainly summarize our representative studies in the 21st Century, and some work from the period 1975–2000 which was not included in our previous account.[1] We have been engaged in research on phthalocyanine (Pc), porphyrin (Por), and cyclodextrin (CDx) systems which show physicochemically intriguing properties, mainly from the standpoints of optical spectroscopy, such as magnetic circular dichroism (MCD), circular dichroism (CD), and electrochemistry. In particular, we have always endeavored to present model systems for the above spectroscopies so that readers can learn how to properly analyze their systems using these powerful and beautiful spectroscopic techniques.

In order to reduce the possibility of wrongly interpreting spectroscopic and electrochemical properties, we have often prepared a series of compounds differing in size and symmetry, and if possible, have always tried to interpret the data conceptually first and then by using molecular orbital (MO) calculations. In exemplary cases, we explained the method of analysis in detail, with a view to instructing organic chemists and biochemists how to analyze their data using our methods.

1. New Subporphyrins and Subphthalocyanines

Phthalocyanines (Pcs) are well-known because of their easy synthesis and robust properties. About 20 years ago, we became interested in finding robust, practical red dyes or pigments, since those known up to that time were weak and faded away with time. Pcs consist of four isoindole units and exhibit blue or green colors, and we felt that if we could create Pc-like compounds consisting of three isoindole units, these might be colored red. On the basis of these thoughts, we checked the Chemical Abstracts, and found that compounds consisting of three isoindole units, presently called subphthalocyanine (subPc) **1** (Scheme 1), were first reported in 1972,[2] and structures were elucidated by X-ray spectroscopy in 1974.[3] From then however, these compounds did not attract the attention of researchers until we published a ring-expansion reaction leading to mono-substituted Pcs in 1990.[4] The following year, we reported the synthesis and properties of a planar subPc dimer containing *t*-butyl groups, but this was a mixture of several isomers.[5] In order to confirm its π structure, we prepared the corresponding totally fluorinated congeners, **2**.[6] This contained two, so-called, cis and trans isomers, and these were separated, crystallized, and analyzed by X-ray spectroscopy. As a result of a cone-shaped C_{3v} structure of the subPc unit, these isomers have either a boat- or chair structure (Figure 1), while spectroscopically, little difference was observed. As shown in Figure 1, the packing structure of the trans isomer reminds us of the wonder of nature. All subPcs prepared to date have a slightly purplish-red color and do not have the vivid red color of oxygen-coordinated blood. Spectroscopically, subPcs are attractive aromatic compounds: although they have cone-shaped structures, they satisfy a $4n + 2$ (where $n = 3$) aromaticity rule, and the electronic absorption spectra can be interpreted in a similar manner to those of smaller azaporphyrin congeners.

The axial OH group of subPc is moderately reactive and can form ether-linkages with other aromatic compounds containing OH groups. When reacted with optically active 1,1′-binaphthol, the optically active subPc dimer, **3**, was formed, which showed a weak exciton coupling interaction of the two subPc units (Figure 2).[7]

As a ring-contracted subPc, subtriazaporphyrin (subAzP), consisting of three pyrrole rings and three *meso*-nitrogen atoms, was reported for the first time by two groups.[8,9] Our subAzP **4** contained six ethyl groups, which affect the spectroscopic properties only marginally, so that we could collect properties

Published on the web June 12, 2009; doi:10.1246/bcsj.82.631

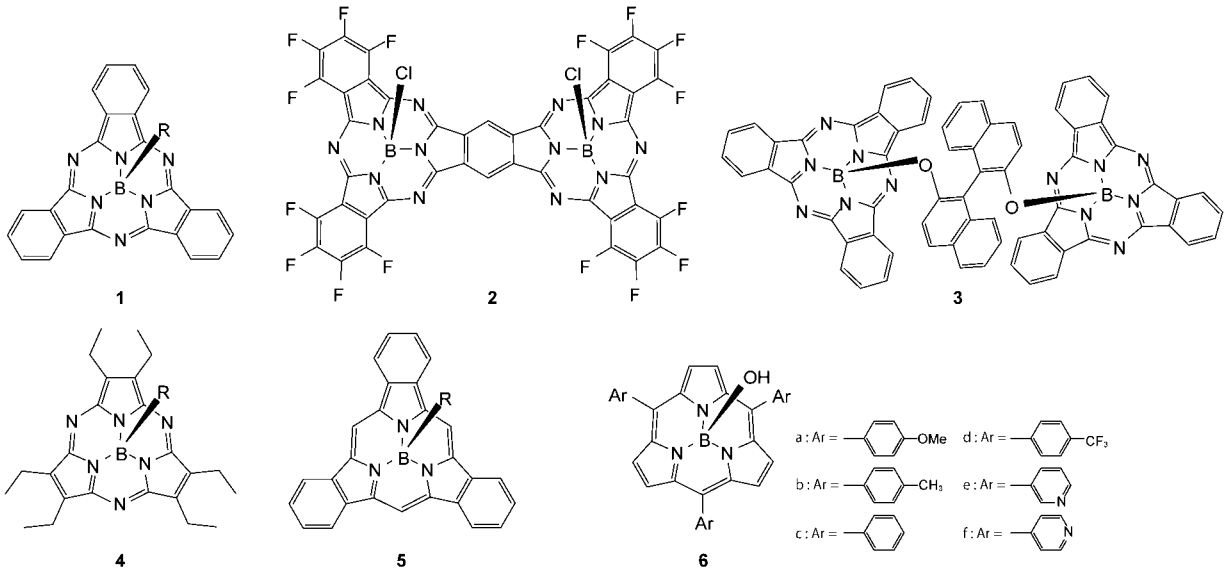

Scheme 1. Structures of some subporphyrins and subphthalocyanines.

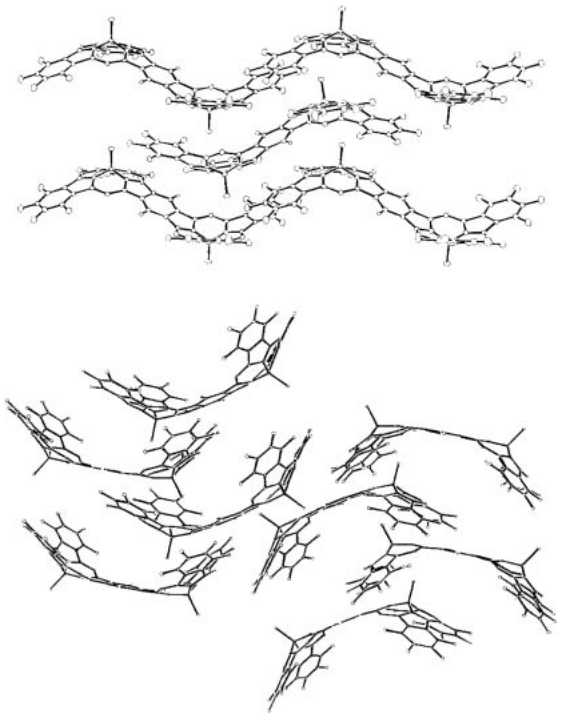

Figure 1. Packing structures of cis and trans isomers of hexadecafluorinated subPc dimer **2**.

inherent to the subAzP skeleton π structure. Both the Q and Soret bands appeared at significantly shorter wavelength than those of the subPcs with concomitant decrease of absorption coefficients, as has been predicted by molecular orbital (MO) calculations.[10] All subPcs and subAzPs reported to date contain boron in their center because of the small size of the central core, and no-one has succeeded in removing the boron.

Following our success in synthesizing subPcs, we became interested in preparing the corresponding porphyrin compounds. We were able to predict their spectroscopic properties from the relationship between Pcs and normal porphyrins, so that our task was then to realize this type of compound and prove the spectroscopic and electrochemical properties. The porphyrin compound corresponding to the subPc structure, **5**, can be named tribenzosubporphyrin (triBsubP). This compound was synthesized in 2006 by Osuka's group[11] in a manner similar to the preparation of tetrabenzoporphyrins (TBP), but using boron salt as a template. A compound which can be called subporphyrin (subP), **6**, was first reported by us in 2007.[12] Our subP compounds with three *meso*-aryl groups could not be synthesized by any method which had been adopted for preparing normal porphyrins. Instead, it was synthesized via tripyrrolylborane as a template (Scheme 2). However, as for normal tetraphenylporphyrins (TPP), the yield increased when benzaldehydes with electron-releasing groups were employed in the last stage of the synthesis, since they attack the electron-deficient α position of pyrrole. The compounds have a cone-shaped structure, as seen for subAzPs.[9] Triaryl-subPs showed Soret- and Q-band-like absorption spectra at around 370–380 and 440–500 nm, respectively (Figure 3). Using MCD spectroscopy, excited-state degeneracy, and small and large angular momentum properties were confirmed for the Soret- and Q-band regions, respectively. It was found that the substituents on the phenyl group affect the spectra significantly:[13] the Q_{00} band intensified with increasing electron-releasing character. Since the electronic absorption bands were found to be explained by four frontier orbitals using MO calculations, the spectra were interpreted by Gouterman's four-orbital theory.[14] The intense Q_{00} band of triarylsubPs containing electron-releasing groups was taken as an indication of a large difference between the HOMO and HOMO$-$1. The HOMO and LUMO have, respectively, three and four nodes, consistent with the $4n + 2$ (where $n = 3$) aromaticity rule. On the other hand, their MCD spectra were not completely elucidated. In particular, the sign sequence in the Soret band region is from minus to plus for compounds with electron-releasing groups, and from plus in ascending energy terms to minus for compounds with electron-withdrawing groups in ascending energy. This type of phenomenon had never been observed in any porphyrin systems reported to date, and still remained unclear. All subP

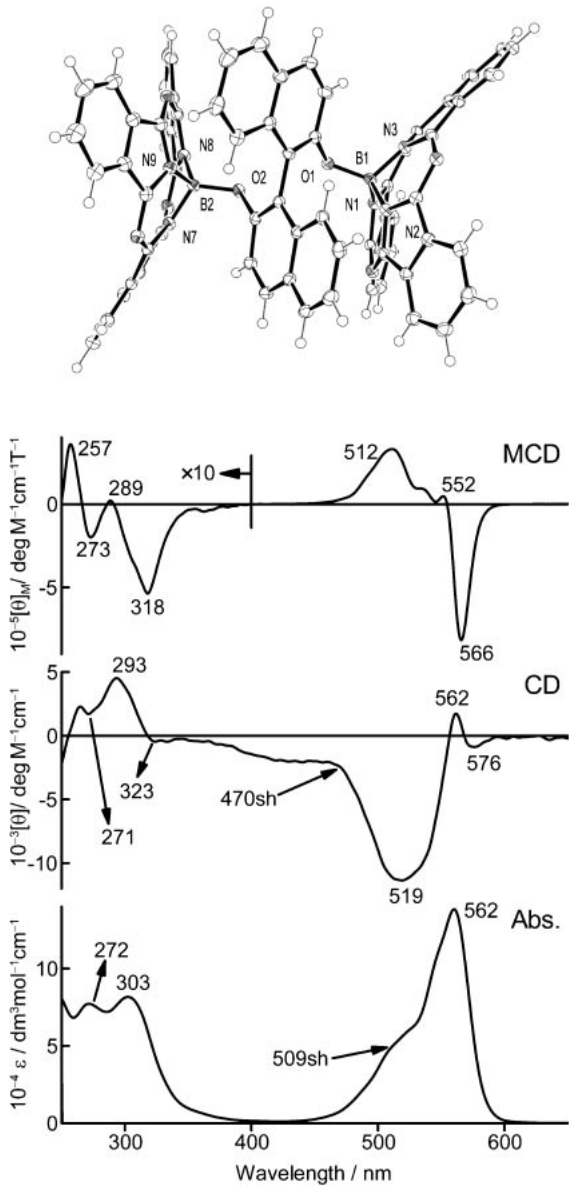

Figure 2. Structure of optically active 1,1′-binaphthyl-linked subPc dimer **3** and its electronic absorption, CD, and MCD spectra.

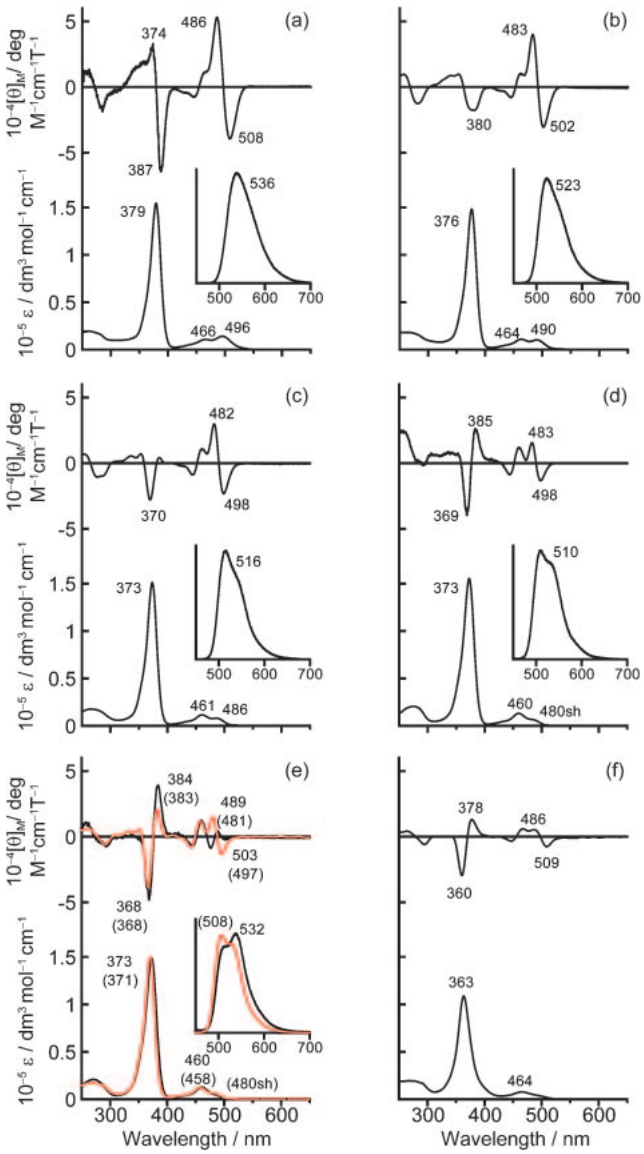

Figure 3. Electronic and MCD spectra of some triphenyl- or tripyridylsubporphyrins. (a) Tri(*p*-methoxyphenyl)-, **6a**; (b) tri(*p*-methylphenyl)-, **6b**; (c) triphenyl-, **6c**; (d) tri(*p*-trifluoromethyl)-, **6d**; (e) tri(3-pyridyl)-, **6e** (dotted lines) and tri(4-pyridyl)-, **6f** (solid lines); and (f) μ-oxo dimer of tri(3-pyridyl)subporphyrin, **6e**. The inset shows the fluorescence spectra.

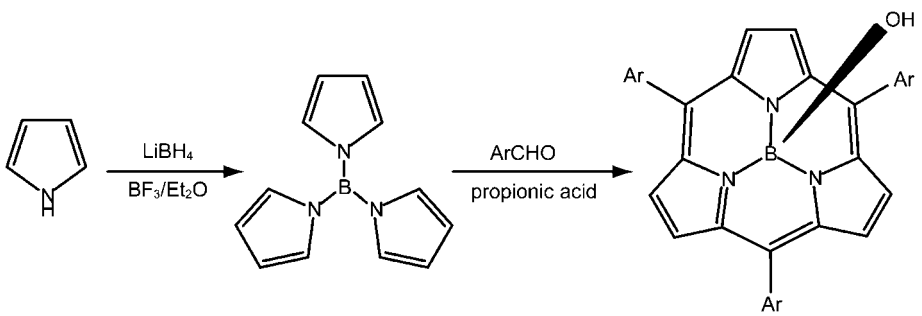

Scheme 2. Route leading to triaryl-subporphyrins.

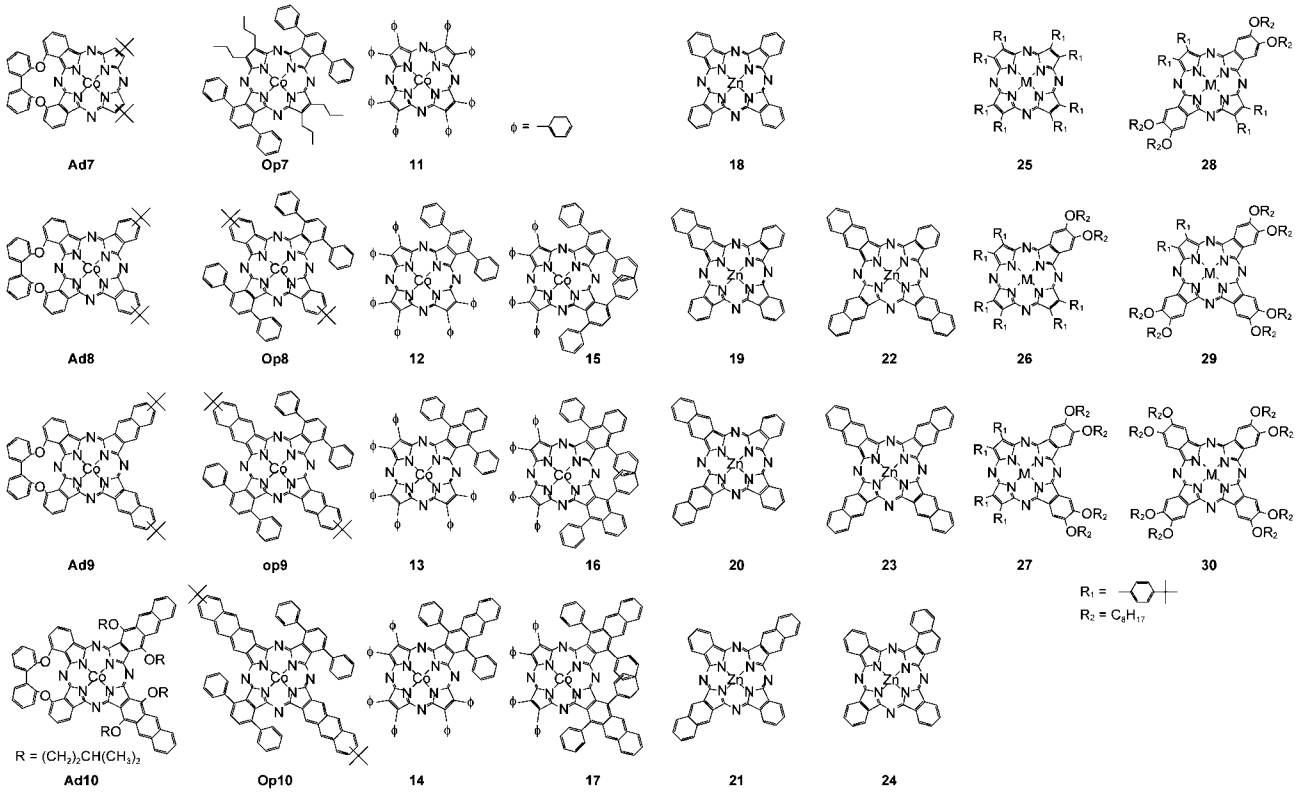

Scheme 3. Structures of low-symmetry tetraazaporphyrins.

compounds showed green fluorescence in the ca. 500–600 nm region, with quantum yields of ca. 0.011–0.012 and 0.06 in benzene and chloroform, respectively.

In agreement with the location of the Soret and Q-bands at shorter wavelength than those of normal tetrapyrrolic porphyrins, the potential difference between the first oxidation and reduction potentials (ca. 2.6 V)[13] was larger than those of normal porphyrins (ca. 2.25 V).[15] These potentials shifted to positive potentials with increasing strength of the electron-withdrawing property of the substituents.

The axial OH group of subP has high reactivity, so that μ-oxo dimers of subP can be obtained easily by dehydration from two subP molecules, or the OH group can be alkoxylated by reaction with alkyl bromide or alkyl chloride at mild temperatures. The absorption peaks were shifted to shorter wavelength by about 10 nm on μ-oxo dimer formation (Figure 3f), consistent with exciton coupling theory.

2. Unsaturated Low-Symmetry Tetraazaporphyrins

The shape and size of porphyrins and tetraazaporphyrins (TAPs) can be tailored by fusing or removing aromatic rings. However, from the spectroscopic point of view, TAPs are more attractive, since the band at the longest wavelength (Q band) has substantial allowed character, and is therefore much stronger. We therefore lowered symmetry of D_{4h} type TAPs by fusing benzene, naphthalene, and anthracene molecules. Two of the same aromatic molecules were fused at adjacent or opposite pyrrole rings of TAPs, leading respectively to compounds of C_{2v} and D_{2h} symmetry, **7**–**10** (Scheme 3).[16a] In this scheme, cobalt complexes were prepared since cobalt complexes of anthracene ring-fused TAPs are known to be stable compared with those containing other metals.[16b] In the case of C_{2v} symmetry, the Q band does not split, but shifts to longer wavelength with increasing molecular size, while in D_{2h} compounds the Q band splits and shifts to longer wavelength (Figure 4), as predicted by symmetry-adapted perturbation theory.[17] In the case of the split Q band, the component at shorter wavelength did not essentially move, but only the longer wavelength component shifted to red with increasing molecular size. The MCD spectra of C_{2v} compounds were dispersion-type corresponding to each absorption peak, since the splitting is small (pseudo Faraday A-term). For D_{2h} compounds, troughs and peaks appeared, associated with the longest and second-longest absorption peaks, respectively, suggesting that the energy difference between the HOMO and HOMO$-$1 (ΔHOMO) is larger than that between the LUMO and LUMO$+$1 (ΔLUMO).[18–20] Interestingly, it was substantiated that the first oxidation of adjacently and oppositely dibenzo-fused cobalt complexes occurs at the central cobalt and the TAP rings, respectively.

Figure 5 shows the spectra of singly aromatic ring-fused molecules **11**–**14** (Scheme 3).[21] Similarly to the doubly oppositely-fused D_{2h} compounds in Figure 4, the Q band splits into two, but the extent increases with increasing size of the fusing aromatic molecules. Of the split Q band, the band at longer wavelength is mainly contributed by the HOMO to LUMO transition, while the HOMO to LUMO$+$1 transition contributes most to the shorter wavelength band. Thus, the splitting of the Q band mainly reflects the extent of splitting between the LUMO and LUMO$+$1.

The effect of lowering the molecular symmetry also appears in the electrochemistry. Figure 6 shows the observed redox

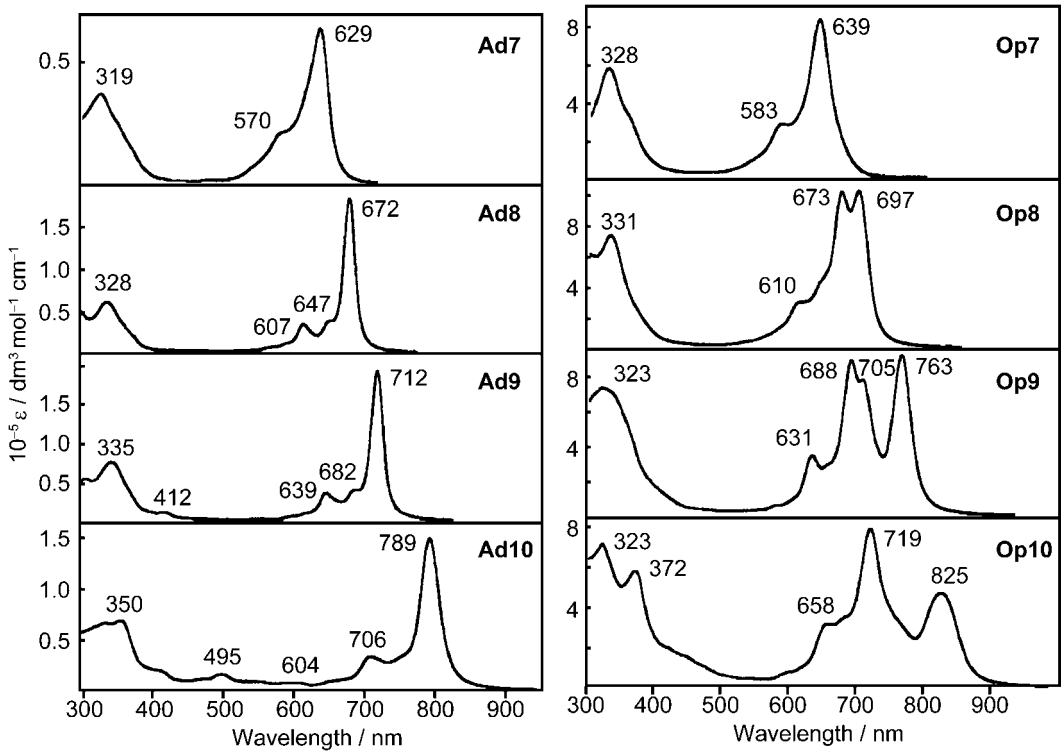

Figure 4. Absorption spectra of a series of C_{2v} (left) and D_{2h} (right) TAPs.

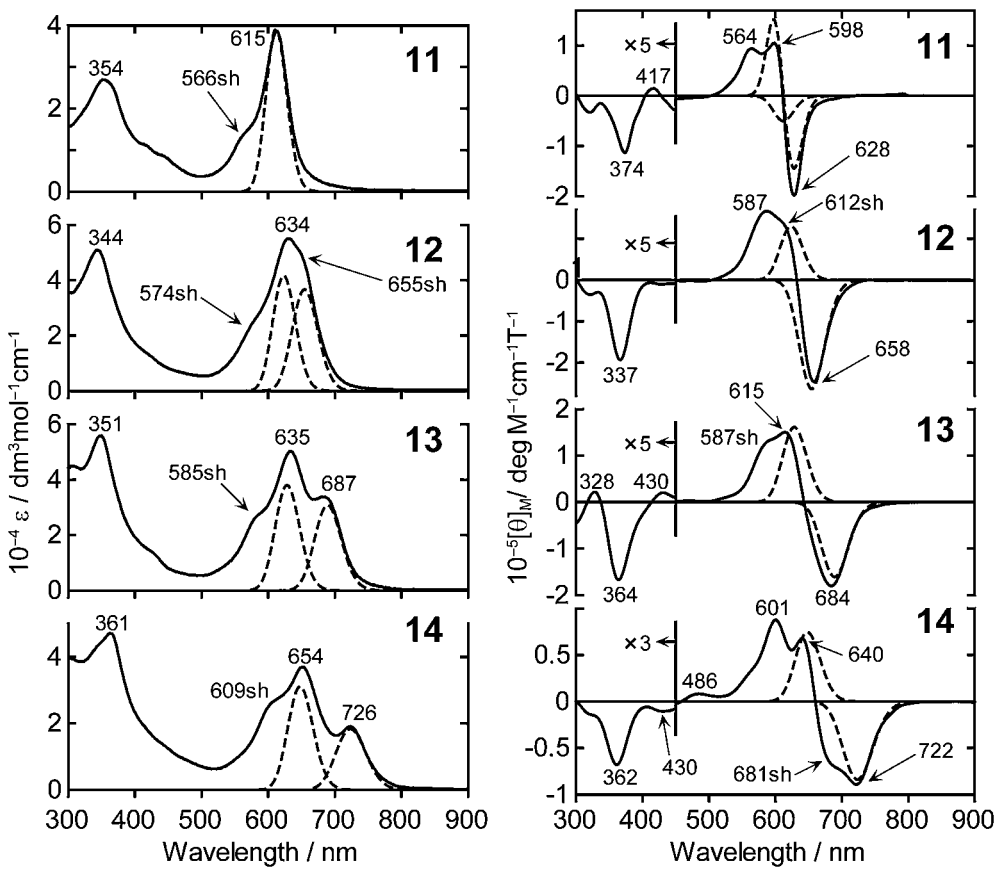

Figure 5. Electronic absorption (left) and MCD (right) spectra of singly aromatic ring-fused C_{2v} cobalt species **11**–**14**.

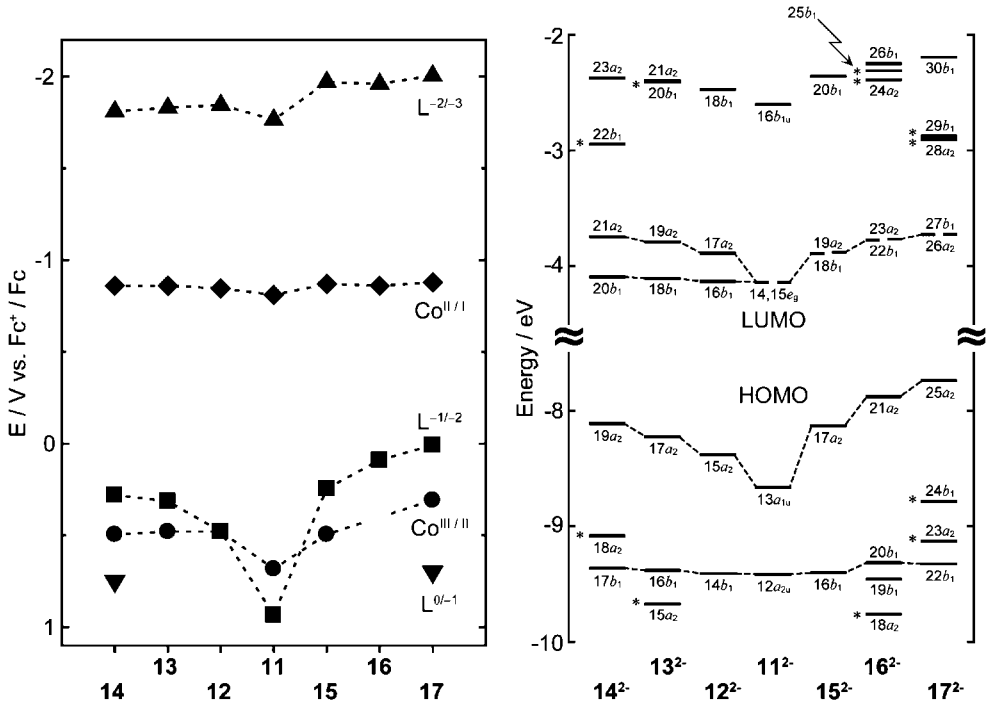

Figure 6. Observed redox potentials of singly and adjacently doubly fused TAP molecules (left), and calculated frontier orbitals (right).

couples and calculated energy levels of some frontier orbitals of singly and adjacently doubly fused species **11**–**17** (Scheme 3).[21] The D_{4h} TAP is situated in the center of the abscissa, and singly and doubly aromatic ring-fused compounds are lined up to the left and right, respectively. The redox couples of doubly-fused molecules lie at more negative (or less positive) potentials than those of singly-fused compounds, indicating that the aromatic rings function as electron-releasing groups. In addition, this figure proves that the electron-releasing ability of the aromatic ring increases the larger the size of the molecules. The experimental first oxidation couple is associated with the calculated HOMO level, since the first oxidation is the process which removes one-electron from the HOMO, while the first reduction potential is related to the LUMO, since an electron is added to the LUMO. As can be seen in this figure, the correspondence between the first oxidation and reduction potentials to the HOMO and LUMO, respectively, is very good. Although the LUMO of adjacently di-substituted species is practically doubly degenerate, that of singly-substituted species splits into two levels, and the extent of splitting increases, consistent with the increasing splitting of the Q band of larger aromatic ring-fused TAPs. Although the first oxidation potential of D_{4h} TAP (center) is slightly more positive than expected from the MO calculations, this is due to the oxidation of the central metal (i.e., cobalt). In this particular case, it was elucidated by spectroelectrochemistry that the central cobalt is oxidized from Co^{II} to Co^{III}. As a result, part of the positive charge of the cobalt delocalizes over the TAP molecule, so that the first ligand oxidation of CoTAP becomes more difficult.

Some metal-free versions of the above complexes are also known. Interestingly, two pyrrole protons generally link to the pyrrole nitrogen along the short axes.[22] In the case of the adjacently di-naphtho- and di-benzo-substituted compound (metal-free compound corresponding to Ad**9**), the pyrrole protons linked to both naphthalene- and benzene-fused pyrrole nitrogen are detected at different positions in the ^{1}H NMR spectrum.[23]

Figure 7 shows the ^{1}H NMR spectra of compounds **18**–**24** situated between Pc and naphthalocyanine (Nc).[24] These compounds are important in that there is no peripheral substituent so that they can be used for evaluating the ring currents of large aromatic molecules. Compounds **18**–**24** contain a zinc ion in their center in order to utilise NMR spectroscopy and for ease of separation through coordination of the solvent molecule.

The peripheral protons closest to the center of the molecules appear at the lowest field because of the ring-current effect of the 18π system, and all protons were assigned by the splitting pattern and proton numbers of the signals. The ring currents of Pcs have so far been explained either by a single-loop model regarding the whole macrocycle as a single loop or a five-loop model counting the outer fused benzene rings and central 18π system.[25,26] Although attempts have been made in trying to explain the positions of the proton signals, to date no one has succeeded in explaining the positions of all these low-symmetry compounds.

The electronic absorption spectra of compounds in Figure 7 are shown in Figure 8.[24] As seen in the comparison among Pcs, the adjacently dinaphtho-substituted compound and Nc, the Soret and Q bands shift, respectively, to shorter and longer wavelengths with concomitant increase in intensity with increasing molecular size. The Q band peaks of compound **19** containing three benzene and a naphthalene rings, and of **22** containing a benzene and three naphthalene rings lie, respectively, between Pc **18** and compound **20** with two benzene- and

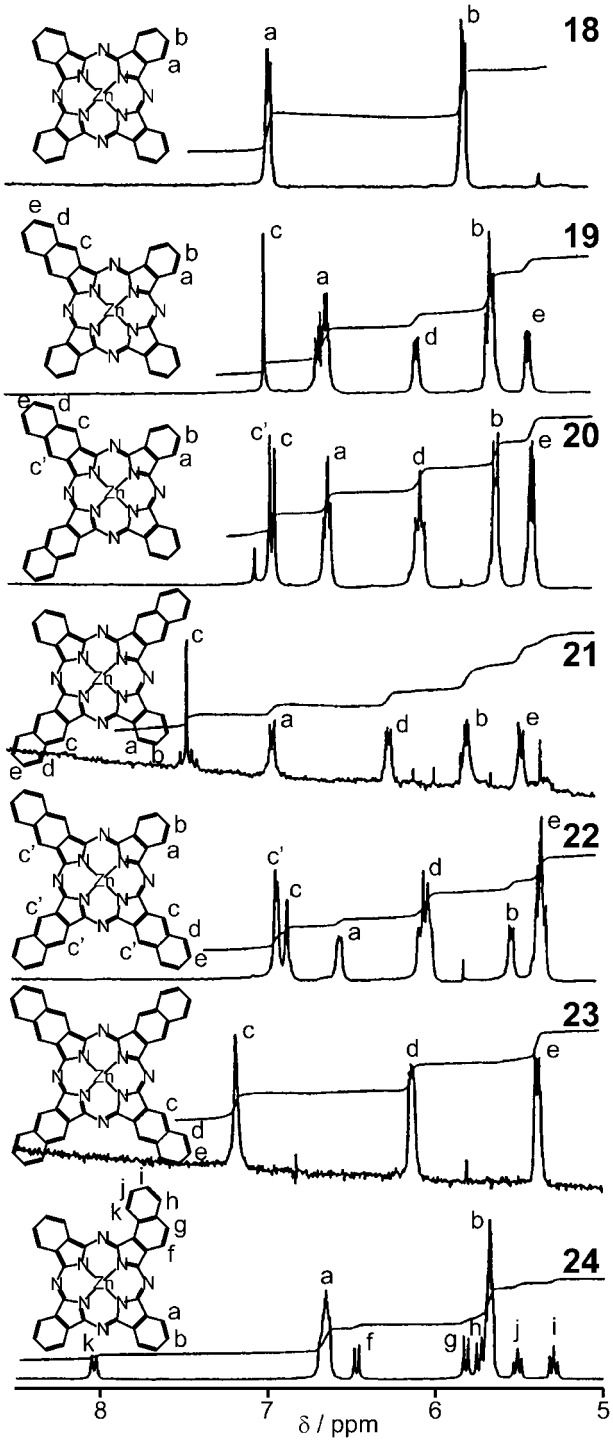

Figure 7. ^{1}H NMR spectra of zinc complexes lying in between Pc and Nc.

two naphthalene rings, and between compound **20** with two benzene- and two naphthalene rings and Nc **23**. Thus, the shift is almost parallel to the size of the molecules. The splitting of the Q band is largest for D_{2h} molecules **21** containing two benzene and naphthalene rings, and the center of the splitting is very close to the peak position of the corresponding adjacent molecule **20**. These observations are reasonably explained by considering symmetry-adapted first order perturbation theory.[17]

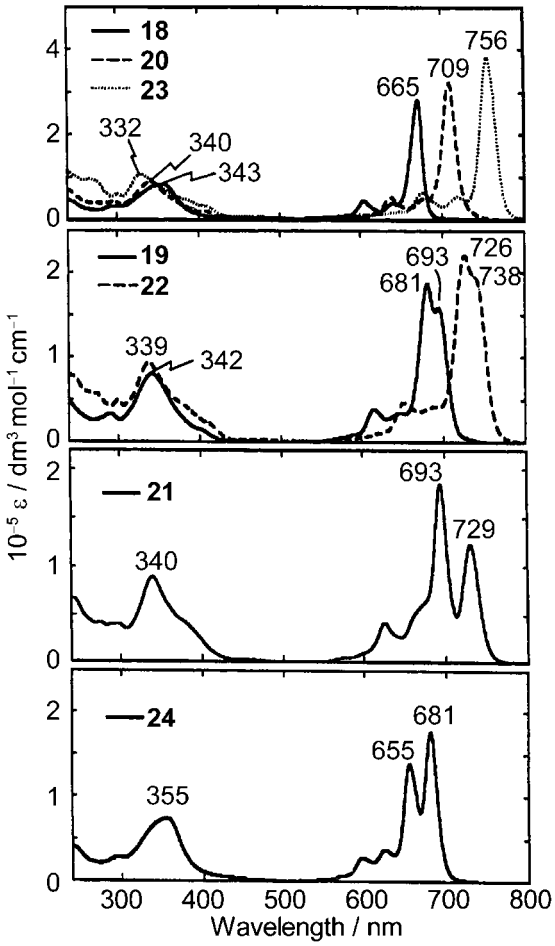

Figure 8. Electronic absorption spectra of zinc complexes lying in between Pc and Nc.

The effect of lowering the symmetry appears more markedly for smaller molecules.[27] Figure 9 shows the calculated and experimental spectra of compounds situated between TAP and Pc (Zn**25**–Zn**30**). Zinc was chosen since we can determine the molecular structure using NMR spectroscopy, while information on the excited states can be obtained by various spectroscopies, including fluorescence and time-resolved EPR. As seen here, the relative position, splitting, and relative intensity ratio of the split Q band are well reproduced by the calculations. Consistent with considerations from group theory,[17] the splitting of the Q band of compounds Zn**26** and Zn**29** containing one and three benzene rings are very close, and the adjacently di-benzo-fused molecule Zn**27** shows a single-peak Q band, reflecting a small degree of splitting (see also the components of the Q band obtained by band-deconvolution).

The redox potentials and calculated molecular orbitals (MOs) of these molecules are summarized in Figure 10. The first oxidation potential becomes less positive with increasing molecular size and the calculated HOMO level changes similarly. The observed first reduction potential seems to change irregularly with molecular size and shape, but these data indicate that the potentials for TAP Zn**25**, mono-substituted Zn**26**, and oppositely di-substituted TAPs Zn**28** are almost identical, while those of adjacently di-substituted Zn**27** and triply-substituted Zn**29** are also very close at different

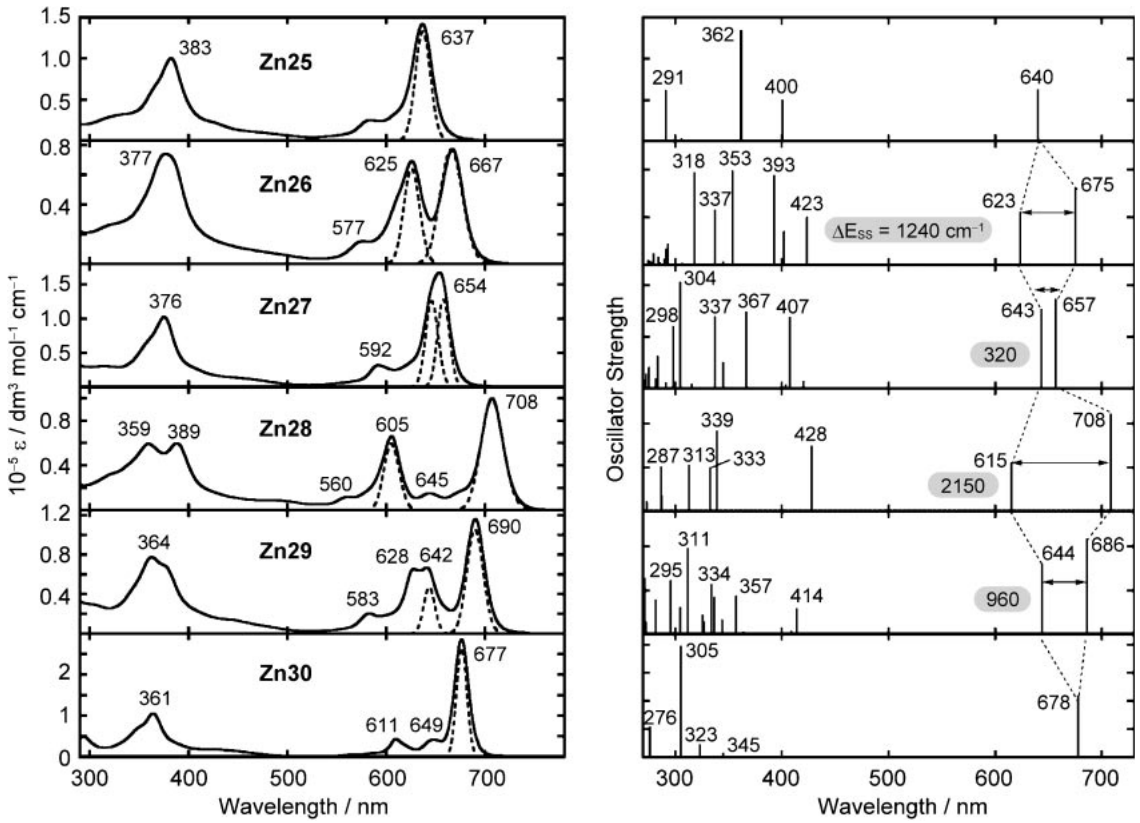

Figure 9. Electronic absorption spectra of TAP compounds situated between TAP and Pc (left) and their spectra obtained by molecular orbital calculations (right). Broken lines in the experimental spectra are Q_{00} (Q_{x00} and Q_{y00}) components obtained by band-deconvolution.

values. Since surprisingly, this irregular tendency of the variation of the first reduction potential was reproduced by MO calculations,[27] we felt that there must be some clue to the origin of this phenomenon in the calculations, and indeed we were able to find the reason (Figure 11). As shown in this figure, the coefficient of the β-carbons of the pyrrole rings of the LUMO is different along the x and y directions. For example, for the e_{gx} orbital, the coefficient along the y axis is much larger than that along the x axis which is practically negligible. Thus, when benzene is fused along the y axis of e_{gx} of TAP, Zn**25**, to produce the singly fused TAP species (Zn**26** in this figure), the LUMO level destabilizes, while the destabilization is negligible when it is fused along the x axis. Therefore, the LUMO level of the singly benzene-fused species, Zn**26**, remains the same as that of TAP (Zn**25**), resulting in marked splitting of the LUMO and LUMO+1. The addition of a second benzene ring results in two isomers, expressed as Zn**27** and Zn**28**. In the former case, both benzene rings are fused on the y axis. Therefore, only the LUMO+1 energy of Zn**26** is destabilized, while the LUMO energy is not influenced by the fused benzo rings. The effect on Zn**27** is clearly very different, since the second benzene ring is fused on the x axis. Compared with Zn**26**, LUMO+1 which originates from the e_{gx} orbital of Zn**25** is barely influenced, while the LUMO is destabilized by the adjacently fused benzene ring. Thus, the LUMO energy is very close to that of LUMO+1 in the case of Zn**26**. In a similar manner, we can essentially explain the same LUMO energy for Zn**27** and Zn**29**.

In the case of the HOMO however, the orbital energy destabilizes with increasing number of fused benzene rings, since the electron density, i.e., the coefficient of the β-carbon of the pyrrole ring is the same, irrespective of the direction of x and y. Thus, the HOMO energies of Zn**27** and Zn**28** are approximately the same.

Porphyrinoids are often used as photosensitizers, particularly in the field of photodynamic cancer therapy.[28–30] When these molecules are photoexcited, the singlet excited states convert to triplet excited states through intersystem crossing, and these species react with triplet oxygen dissolved in our tissue, to generate singlet oxygen which attacks cancer tissue. Thus, the elucidation of the excited state properties and a high-yield for production of singlet oxygen are important for researchers in the field of phototherapy. We have succeeded[31] in collecting fluorescence, phosphorescence (Figure 12), and time-resolved EPR data of the metal-free, zinc, magnesium, and palladium derivatives of **26**–**30**, and examined how the singlet oxygen yield varies depending on the molecular size and symmetry (Table 1 and Figure 13). Thus, the lowest singlet (S_{1x} and S_{1y}) and lowest triplet excited state (T_{1x}) energies were quantitatively determined from the electronic absorption and phosphorescence spectra, respectively, while the second lowest triplet state (T_{1y}) was evaluated by using the energy splitting between T_{1x} and T_{1y} obtained for the zinc complexes Zn**25**–Zn**30**[27] shown in Figure 9 (Figure 14). The singlet oxygen quantum yields (Φ_Δ) were strongly dependent on the π-conjugated system (Figure 13). In particular, while the Φ_Δ value of H_2**27** is

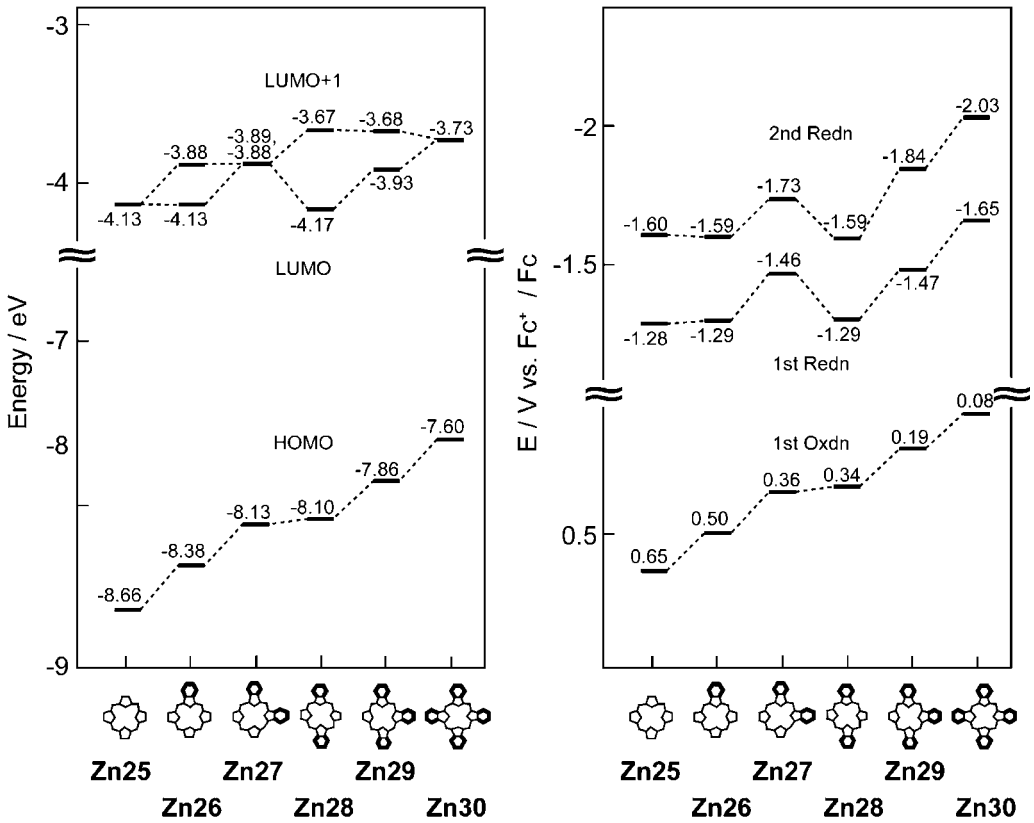

Figure 10. Calculated energy levels of some frontier orbitals (left) and experimental redox potentials (right) of the compounds situated between TAP and Pc.

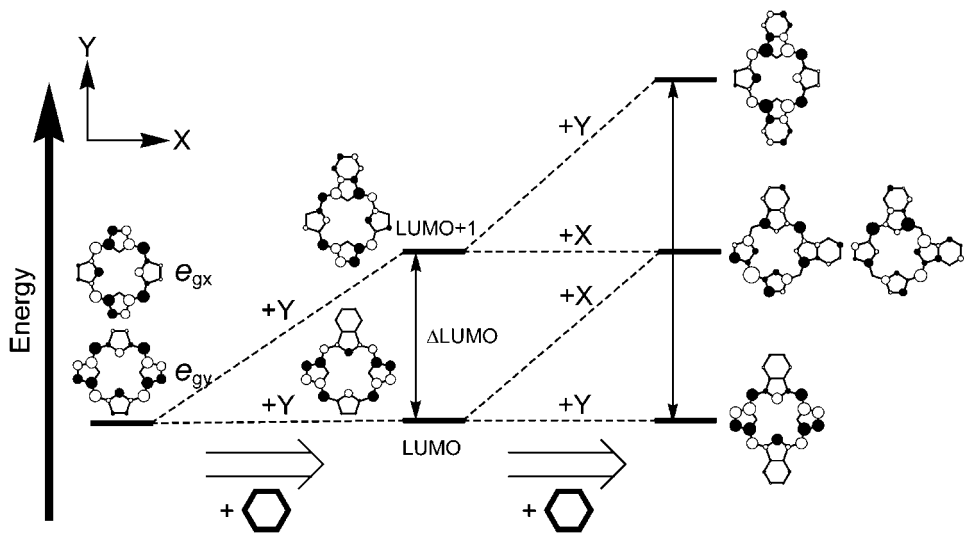

Figure 11. The two LUMOs of TAP and the effects of the number and location of fused benzene rings on the LUMO and LUMO+1 energies. Note, although not shown, that the coefficient of the β-carbon of the pyrrole rings is the same irrespective of the direction for the HOMO, while that of the e_{gx} and e_{gy} is quite different in the x and y directions. In the case of e_{gx}, for example, the coefficient along the y direction is much larger than that along the x direction.

the smallest, that of H_2**28**, an isomer of H_2**27**, was larger than that of Zn**30**, exceeding the heavy atom effect. That is, the Φ_Δ value increased with increasing splitting of the Q-band. The relationship between the molecular structure and Φ_Δ values can be further transformed into a relationship between the $S_{1x}\cdots T_{1y}$ intersystem crossing rate constant (k_{ISC}) and the energy difference between the S_{1x} and T_{1y} states (ΔE_{SxTy}). In each of the Zn, Mg, and metal-free compounds, the Φ_Δ/τ_F values (τ_F: fluorescence lifetime), which are related to the k_{ISC} values, were proportional to $\exp(-\Delta E_{SxTy})$ (Figure 15), indicating that singlet oxygen ($^1\Delta g$) is produced via the T_{1y} state and that the $S_{1x} \rightarrow T_{1y}$ process follows the energy gap law.

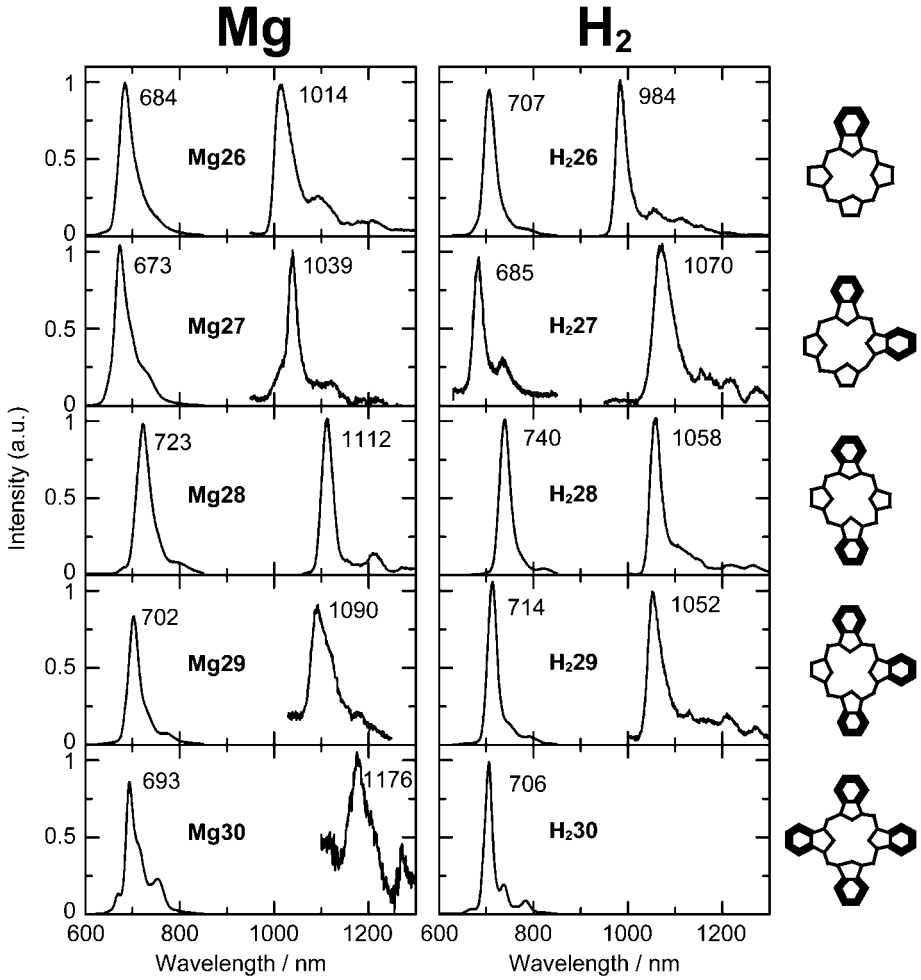

Figure 12. Luminescence spectra of Mg (left) and metal-free (right) derivatives of low-symmetry TAP compounds.

Table 1. Fluorescence Lifetimes (τ_F) and Singlet Oxygen Yields (ϕ_Δ)

Compounds	τ_F/ns	ϕ_Δ[a)]	ϕ_Δ/τ_F 10^{-8} s
Zn**26**	1.5	0.62	4.2
Zn**27**	2.2[b)]	0.49	2.2
Zn**28**	1.1[b)]	0.60	5.3
Zn**29**	1.5	0.55	3.6
Zn**30**	3.4	0.43	1.3
Mg**26**	2.5	0.27	1.1
Mg**27**	3.8	0.18	0.48
Mg**28**	2.6	0.24	0.91
Mg**29**	3.4	0.20	0.61
Mg**30**	6.5	0.14	0.21
H_2**26**	1.7	0.23	1.4
H_2**27**	0.081	0.010	1.3
H_2**28**	2.4	0.50	2.0
H_2**29**	4.2	0.27	0.64
H_2**30**	6.1	0.14	0.24

a) ϕ_Δ measurements were carried out with various laser powers, and the average τ_F values were employed. The experimental errors were within 15%. b) These values were erroneously reported oppositely in our original paper (Ref. 31).

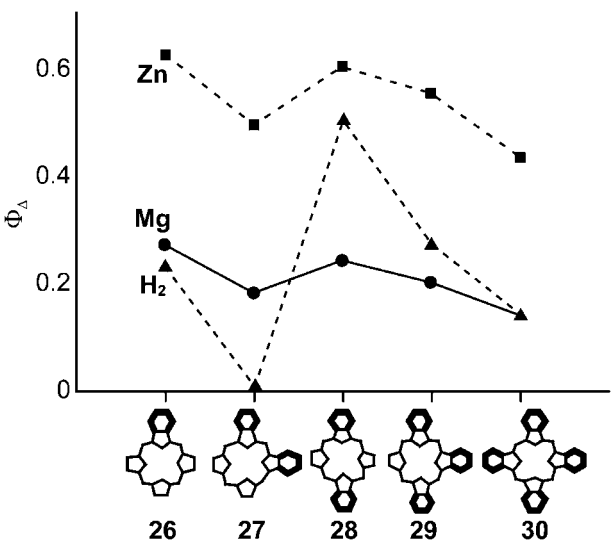

Figure 13. Relationships between the molecular structures of low-symmetry TAPs and Φ_F.

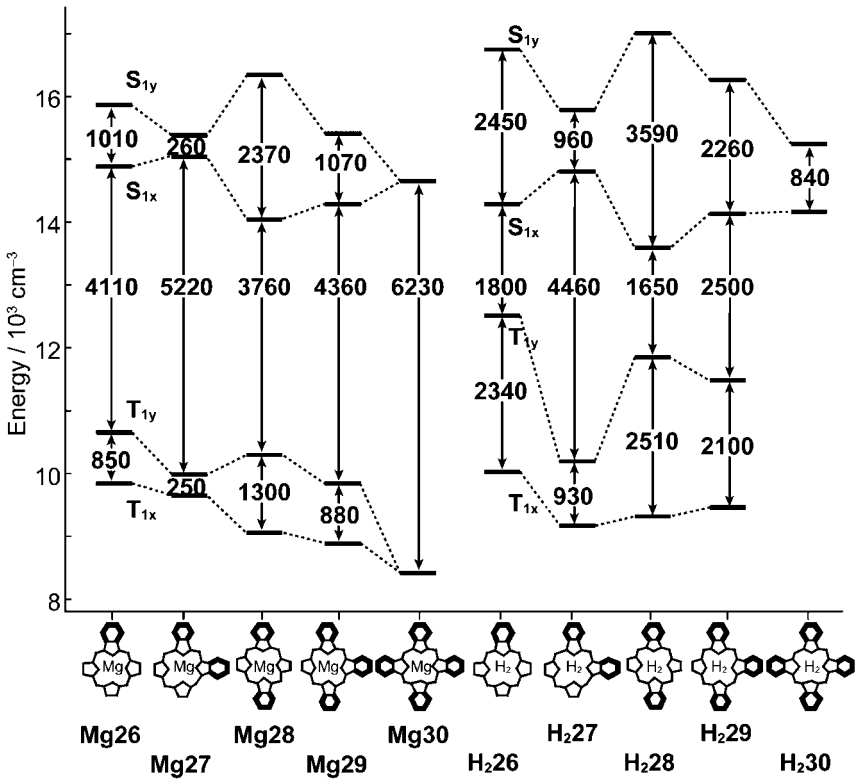

Figure 14. Summary of the ΔE_{SS} and ΔE_{TT} values of Mg (left) and metal-free (right) compounds.

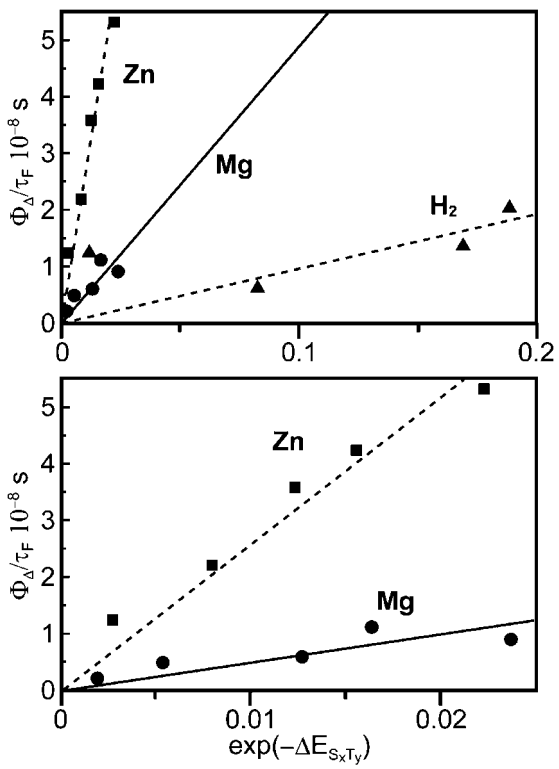

Figure 15. Relationship between the Φ_Δ/τ_F and $\exp(-\Delta E_{SxTy})$ values of the low-symmetry TAPs. The ΔE_{SxTy} value is in k cm^{-1}.

Minor prototropic tautomers of H_2**26**, H_2**27**, H_2**28**, and H_2**29** were detected in the electronic absorption and MCD spectra.[32] The presence of two prototropic tautomers of H_2**26** and H_2**29** were proven by the combined use of CI calculations.

Adjacent-type Pc compounds containing electron-donating and -withdrawing groups are attractive from the standpoint of nonlinear optics. However, the condensation reaction between phthalonitriles containing electron-withdrawing (A) and -donating groups (D) generally produces only Pcs with electron-withdrawing groups or those with three electron-withdrawing groups and one electron-donating group, due to the higher reactivity of phthalonitriles with electron-withdrawing groups. We overcame this by first connecting two phthalonitrile units with electron-releasing character at higher temperature, and then by introducing phthalonitrile with electron-withdrawing groups at lower temperature. In this way, AADD type Pcs were prepared preferentially.[33]

3. Hydrogenated Low-Symmetry Tetraazaporphyrins

In order to determine the relationships between the molecular structure and spectroscopic and electrochemical properties, the effect appears more clearly the smaller the molecule. Accordingly, following aromatic ring-fused low symmetry compounds, we decided to examine hydrogenated TAPs. Hydrogenated TAPs were first synthesized by Linstead et al. in 1958,[34] but these compounds were not well elucidated because of the tendency to return to unsaturated TAPs or even to degradated products. In 2000, this problem was overcome by Makarova, Luk'yanets, et al., by introducing bulky substituent groups which prevent coplanarization of two C–H bonds at adjacent pyrrole β-carbons.[35] Further, several years later, a

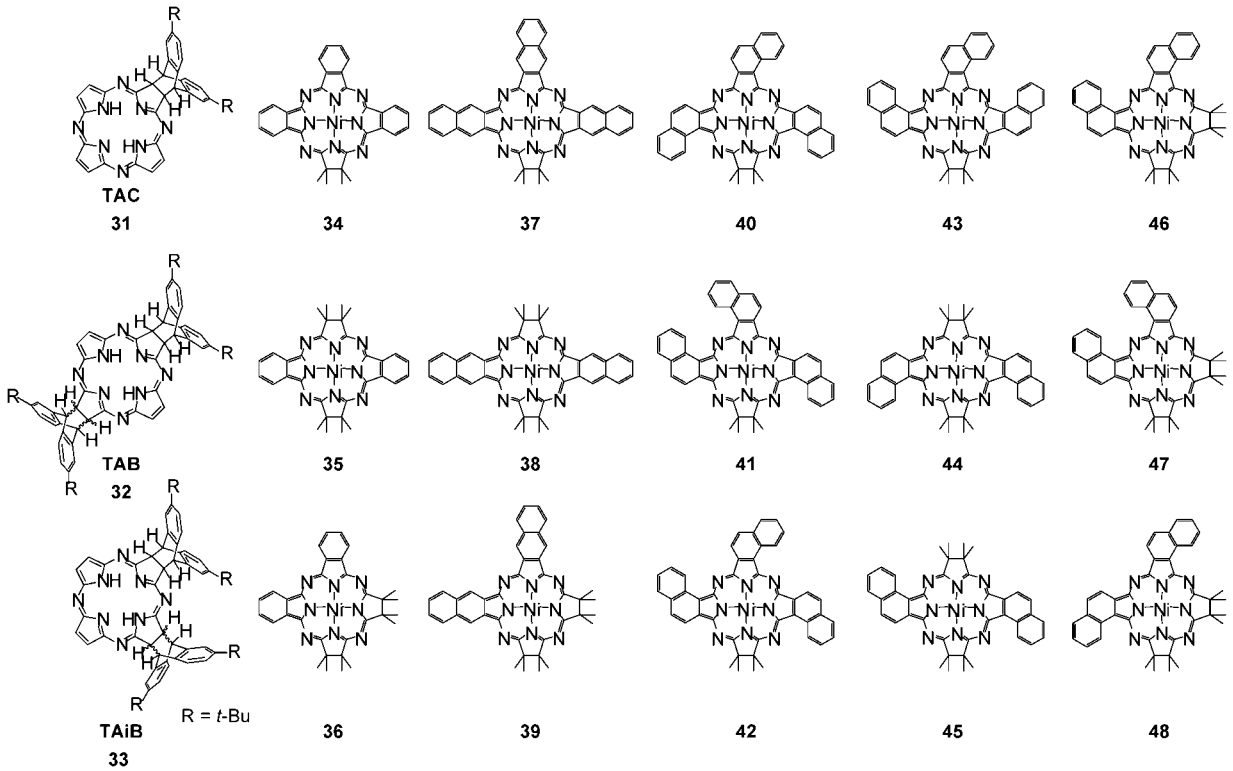

Scheme 4. Structures of hydrogenated tetraazachlorins, -bacteriochlorins, and -isobacteriochlorins.

series of these metal-free compounds were characterized using several spectroscopic methods and calculations.[36] The TAPs containing one and two hydrogenated pyrrole rings are called tetraazachlorin (TAC) **31** (Scheme 4), and tetraazabacteriochlorin (TAB, trans type) **32** or tetraazaisobacteriochlorin (TAiB, cis type) **33**, respectively. Since the molecules are the smallest of the tetrapyrrolic porphyrins, the effect of lowering the symmetry appeared most profoundly among the porphyrins reported to date. The potential difference between the first oxidation and reduction couples decreases in the order TAP > TAiB **33** > TAC **31** > TAB **32**. The splitting of both the Q and Soret bands decreases in the order TAB **32** > TAC **31** > TAP > TAiB **33**. In particular, the splitting of the Q ($9900\,cm^{-1}$) and Soret bands ($5685\,cm^{-1}$) of TAB **32** is the second largest seen in the porphyrins reported to date. The MCD spectral pattern was always minus-to-plus in ascending energy, indicating that the ΔHOMO is larger than the ΔLUMO. These electrochemical, absorption, and MCD properties were well reproduced by MO calculations. According to the calculations, the HOMO and LUMO+1 destabilized on going from TAP to TAC **31** and further to TAB **32**, while the HOMO−1 and LUMO levels remained almost unchanged. This can be explained, since in TAP, the HOMO and LUMO+1 have some coefficient on the pyrrole rings that are hydrogenated in TAC **31** and TAB **32**, while the LUMO and HOMO−1 have very small coefficients. The shapes of the LUMO and LUMO+1 of TAiB **33** differ from those of the other compounds in having no nodal plane on the pyrrole nitrogen atoms, so that their energy changes could not be explained by the same mechanism as in TAC **31** and TAB **32**. However, in agreement with the theoretical prediction,[17] the splitting of the LUMO and LUMO+1 of TAiB **33** was calculated to be very small.

The excited state properties also varied markedly. On going from TAP to TAC **31** and further to TAB **32**, the fluorescence quantum yield decreased by one order in each step. The zero-field splitting parameters D and E of the excited triplet state decrease and increase, respectively, on going from TAP to TAC **31** and further to TAB **32**, although the values for TAiB **33** were larger than those of the other species. The parameter D reflects an anisotropic distribution of unpaired electrons towards the out-of-plane axis (z axis) with respect to the distribution in the ring plane (x, y axes). Therefore, the decrease in D on going from TAP to TAB **32** was the opposite behavior to that expected for delocalization of π electrons, although similar results were reported for normal porphyrin systems before our report.[37] In general, the T_1 states of Pcs and porphyrins without transition metals are treated as a single configuration of the HOMO–LUMO transition, where the zero field splitting is interpreted through spin–spin interactions between the HOMO and LUMO electrons. Since there are almost no π electrons on the reduced pyrrole moiety, while the π electron density in the other regions of the HOMO simultaneously increases, the spin over the unreduced moiety of the HOMO interacts with the spin over the LUMO, and thus increases the D value. On the other hand, the absence of interaction between the spin over the reduced pyrrole moiety of the HOMO and the spin over the LUMO leads to a decrease in D value. The decreasing D value was therefore taken to be an indication that the latter contribution to the D value is more important. The parameter E reflects an anisotropic distribution of unpaired electrons towards the in-plane axes x and y, so that

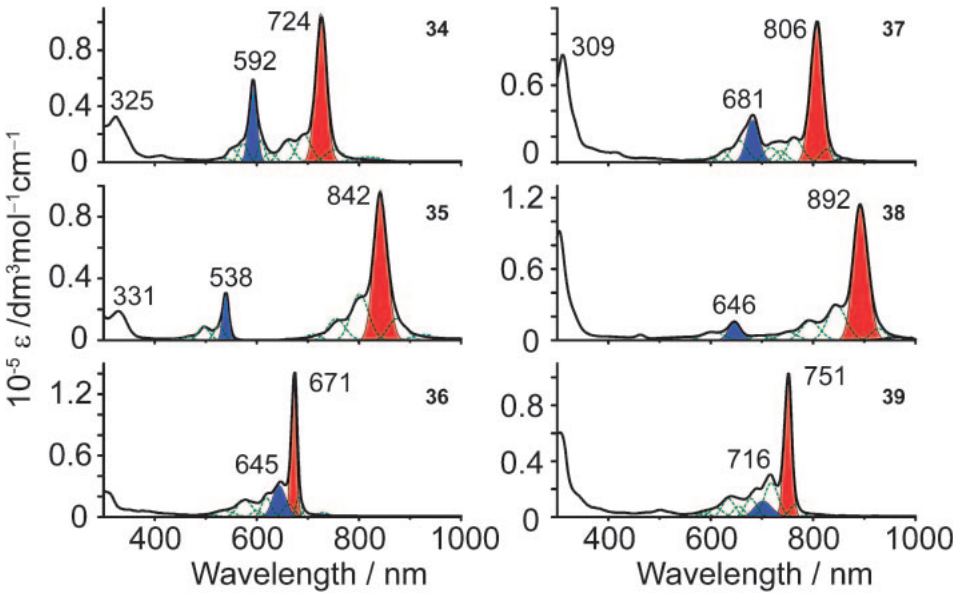

Figure 16. Electronic absorption spectra of benzo- (left) and 2,3-naphtho-substituted (right) TAC (top), TAB (center), and TAiB (bottom) (for structures of the compounds, see Scheme 4).

the observed increase in E was explained by symmetry lowering. The above changes of D and E values were quantified by calculations under a half-point-charge approximation.

This research was further extended to benzo- or 2,3-naphtho-fused metallo-TAC, -TAB, and -TAiB derivatives **34–39** (Scheme 4).[38] These compounds were obtained by a template reaction using nickel salt (as another metal, only the VO ion was possible), and their electronic absorption spectra are shown in Figure 16, together with Q_x and Q_y components obtained by band deconvolution of both absorption and MCD spectra. Interestingly and unexpectedly, the splitting of the Q bands of 2,3-naphtho-fused species is always smaller than that of the corresponding benzo-substituted derivatives. Since the splitting is generally larger for compounds whose x/y ratio is larger, this result was a surprise and the reason has not yet been resolved, although molecular orbital calculations reproduced the observation that the splitting of naphtho-fused derivatives is smaller. The spectra of isomeric benzo-substituted D_{2h} NiTAB **35** and C_{2v} NiTAiB **36** on oxidation to ring-oxidized cation radicals were also recorded for the first time. In the former case, the split Q band peaks shifted from 842 and 538 to 1054 and 584 nm, respectively, while in the latter case, Q- and Soret bands originally at 671 and 313 nm appeared at 850 and 512 nm, respectively, suggesting a decrease in the HOMO–LUMO (LUMO+1) and HOMO−1–LUMO (LUMO+1) energy gap.

One of the most prolific areas for these compounds was in the IR spectra and their characterization by MO calculations. As seen in Figure 17, it is now possible to discriminate between adjacent and opposite isomers by IR spectra, and the peak intensity and positions of the spectra can be almost perfectly reproduced. This conversely means that we can estimate the IR spectra of low-symmetry porphyrinoids before measuring their IR spectra, and further that vibrational CD can also be predicted for optically active porphyrinic compounds.[39]

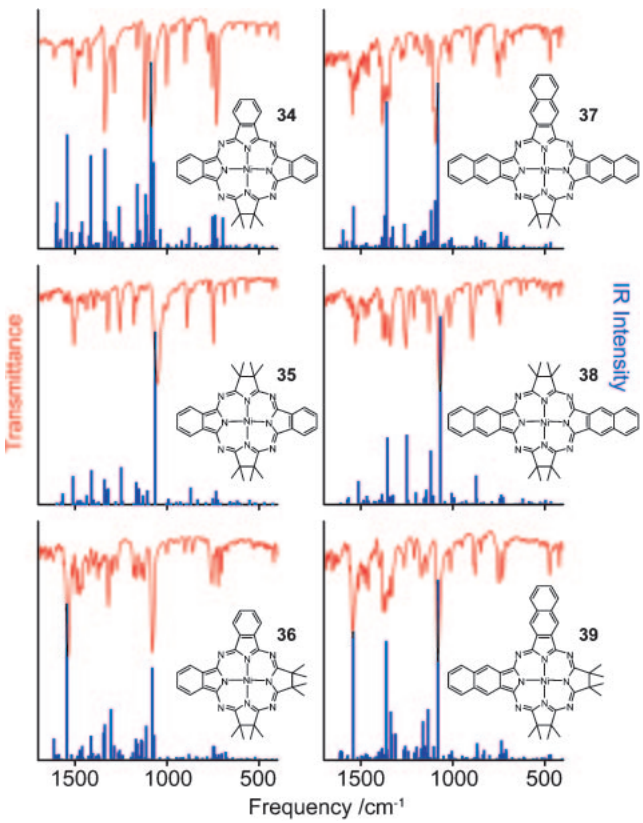

Figure 17. Experimental and calculated IR spectra of benzo-substituted (left) and naphtho-substituted (right) NiTAC (top), NiTAB (center), and NiTAiB (bottom).

Since dehydrogenation does not occur easily, the oxidation and reduction potentials were recorded at least up to the second step for all VO and Ni compounds, and occasionally the third oxidation and reduction steps were also determined for some compounds.

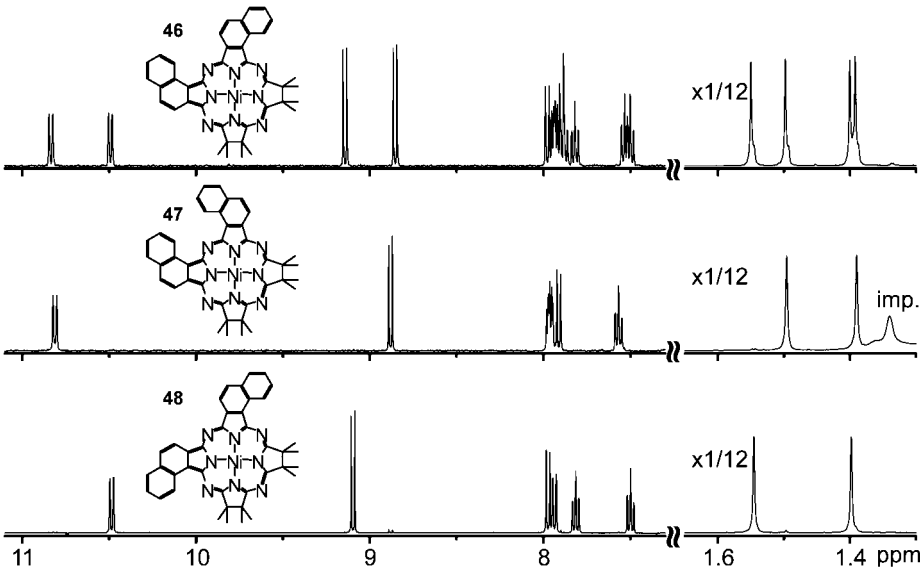

Figure 18. ^{1}H NMR spectra of three isomers of 1,2-naphtho-fused TAiBs **46**–**48**.

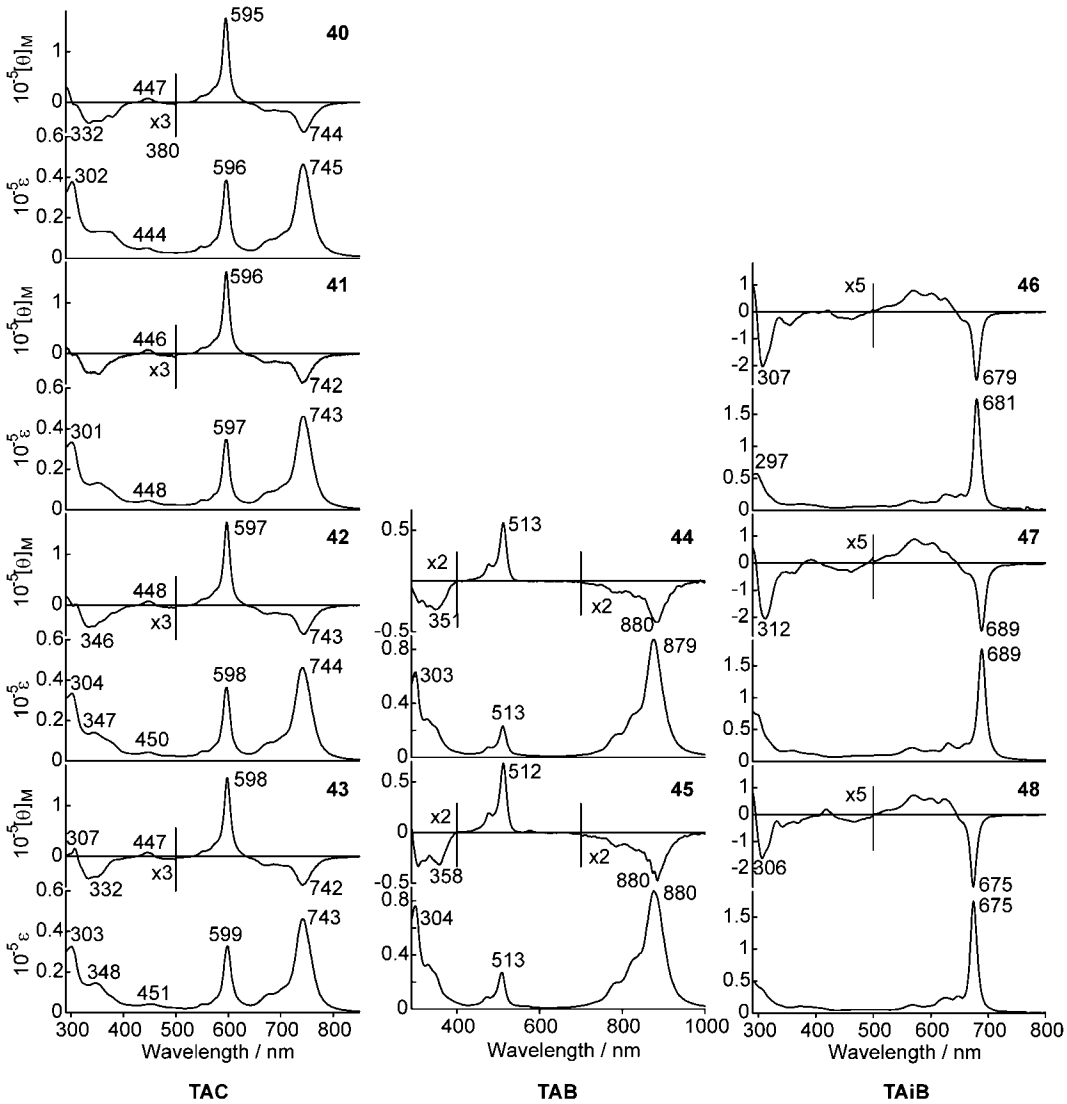

Figure 19. Electronic absorption and MCD spectra of compounds **40**–**48**.

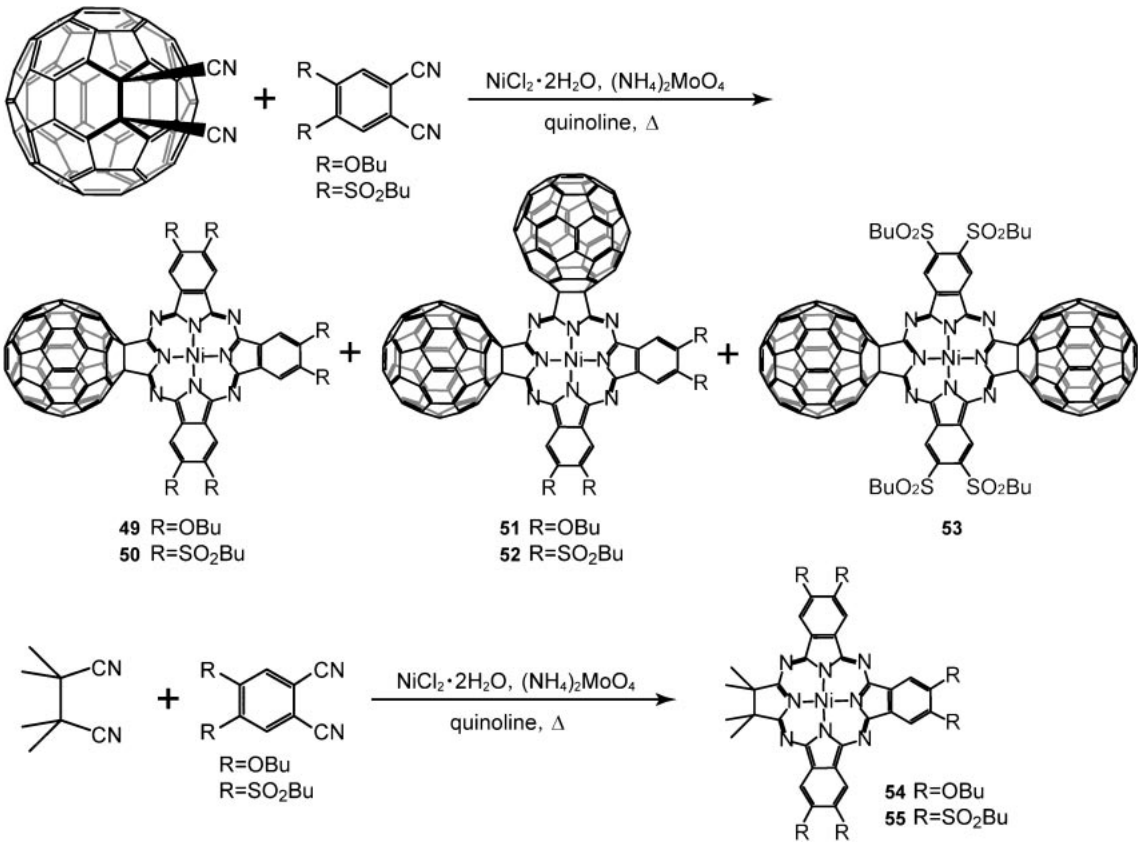

Scheme 5. Route leading to fullerene-linked hydrogenated TAC, TAB, and TAiB, and the corresponding compounds without fullerene.

Following the above aromatic ring-fused hydrogenated species, we explored the synthesis, separation, and characterization of hydrogenated TAP compounds obtained by mixed condensation of tetramethylsuccinonitrile and 1,2-dicyanonaphthalene or naphthalene-1,2-dicarboximide plus urea.[40] As shown in Scheme 4, isomers **40**–**48** can be produced by the reaction, but all compounds could be separated and characterized properly. For the identification of the compounds, ^{1}H NMR and mass spectroscopy was intensively utilized. When isomers were not discriminated by these methods, even yields were taken into account, since isomers which have stronger repulsion between the naphthalene units were always produced in lower amounts. Figure 18, for example, shows the ^{1}H NMR spectra of three isomers of di-1,2-naphtho-fused tetraazaisobacteriochlorin **46**–**48**. Two naphthalene molecules face either outward (bottom) or inward (middle), while both outward and inward (top), and the spectra at the top can be expressed by superimposition of the spectra at the middle and bottom. Figure 19 shows the absorption and MCD spectra of all the compounds. Spectroscopic differences as a result of the varying orientation of the naphthalene molecules are small, although those between TACs **40**–**43**, TABs **44** and **45**, and TAiBs **46**–**48** are marked. The small difference due to the different orientation of naphthalene was reproduced in the MO calculations. Thus, the absorption band position of the isomers which show experimental absorption bands at slightly shorter wavelength than other isomers was calculated at slightly shorter wavelength. In this way, the data in Figure 19 are important in that a series of many structural isomers are collected. Experimental IR spectra of these compounds were also well reproduced in position and relative intensity, so that it is now possible to distinguish between these isomers using IR spectroscopy.

In order to control the communication between substituents and the hydrogenated TAP core, TAC-, TAB-, and TAiB compounds linked with fullerene (C_{60}) were prepared by mixed condensation of dicyanofullerene and phthalonitrile derivatives with either electron-donating (butoxy) or electron-withdrawing (butylsulfonyl) groups.[41] From the reaction mixture, TAC with one fullerene **49** and **50**, TAiB **51** and **52**, and TAB **53** with two fullerene molecules were separated (Scheme 5). In order to extract the role of the fullerene unit, the corresponding compounds without fullerene units were also prepared similarly (Scheme 5). Figure 20 compares the spectra of a fullerene-linked TAC and the corresponding compounds without fullerene, **54** and **55**. Of the four compounds, three compounds show spectra of a similar pattern, with two sharp Q absorption bands and a corresponding minus-to-plus MCD pattern in ascending energy. Only the absorption spectrum of TAC with a fullerene and electron-donating group, **49**, showed split peaks corresponding to the Q absorption band at the longest wavelength of the other compounds. In order to understand the electronic structures of the complexes, the MOs and the excitation energies were therefore calculated (Figures 21 and 22). Since the fullerene was linked to the TAC skeleton via sp^3 carbon, dimethylfullerene was used as a constituent unit, and

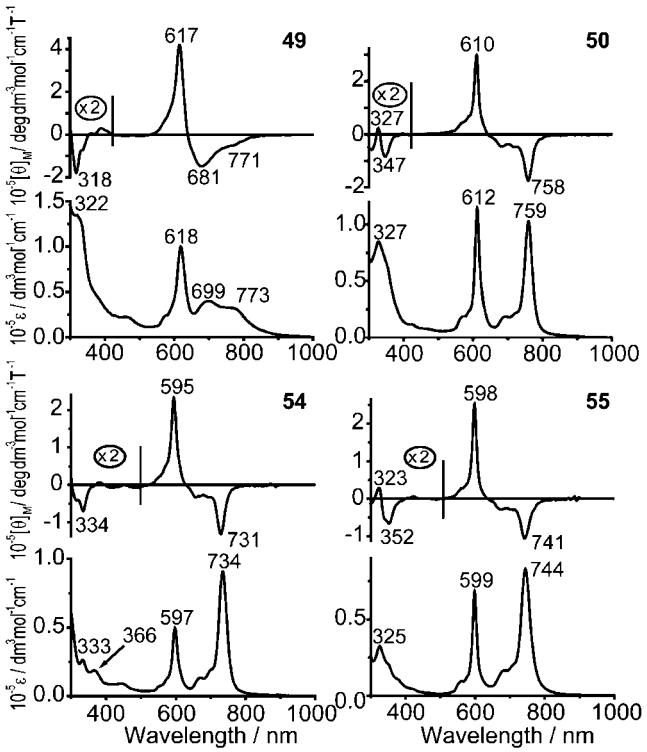

Figure 20. Absorption and MCD spectra of one-fullerene-linked TAC with butoxy substituents **49** (top left) and butylsulfonyl substituents **50** (top right), and TAC without a fullerene unit but with butoxy substituents **54** (bottom left) and butylsulfonyl substituents **55** (bottom right).

the butoxy and butylsulfonyl substituent groups on the periphery of TAC were replaced by OMe and SO_2Me groups, respectively. As demonstrated in Figures 21a and 22a, the MO energies and distribution of the MO coefficients of TAC–C_{60} strongly reflect those of the TAC and C_{60} components. For example, the HOMO and LUMO of TAC–C_{60} originate from the HOMO of TAC and LUMO of 1,2-Me_2C_{60}, respectively, i.e., the MO coefficients of the HOMO and LUMO of TAC–C_{60} are almost identical to the HOMO of TAC and the LUMO of 1,2-Me_2C_{60}, respectively. This type of localized MO is predicted for most of the MOs of TAC–C_{60}. The HOMO−1 to HOMO−4 are dominated by the low-lying C_{60} orbitals. The calculations also predict that some of the MOs are delocalized over the entire complex. The LUMO+1 and LUMO+2 are of this type, and can be expressed as a linear combination of the LUMO+1 of 1,2-Me_2C_{60} and the LUMO of TAC. This kind of interaction is only observed when the two components are in close enough proximity and have the same symmetry. In other words, the initial LUMO of TAC splits into two delocalized orbitals in the presence of the C_{60} unit. As a consequence, the two weak Q absorption bands of TAC–C_{60} with R = butoxy, **49**, (Figure 20, top left) can be assigned mainly from the HOMO to LUMO+1 and LUMO+2 transitions, respectively. The third sharp band is then assigned as a transition from the HOMO to LUMO+4.

It was found recently that a change of central metal also affects the MO energy of this type of compound.[42]

4. Deformed Phthalocyanines

As deformed porphyrinoids, regular porphyrins whose two pyrrole rings at opposite positions are connected by short alkyl chains and/or those having many bulky substituent groups, have been studied for more than 30 years,[43a] and today two

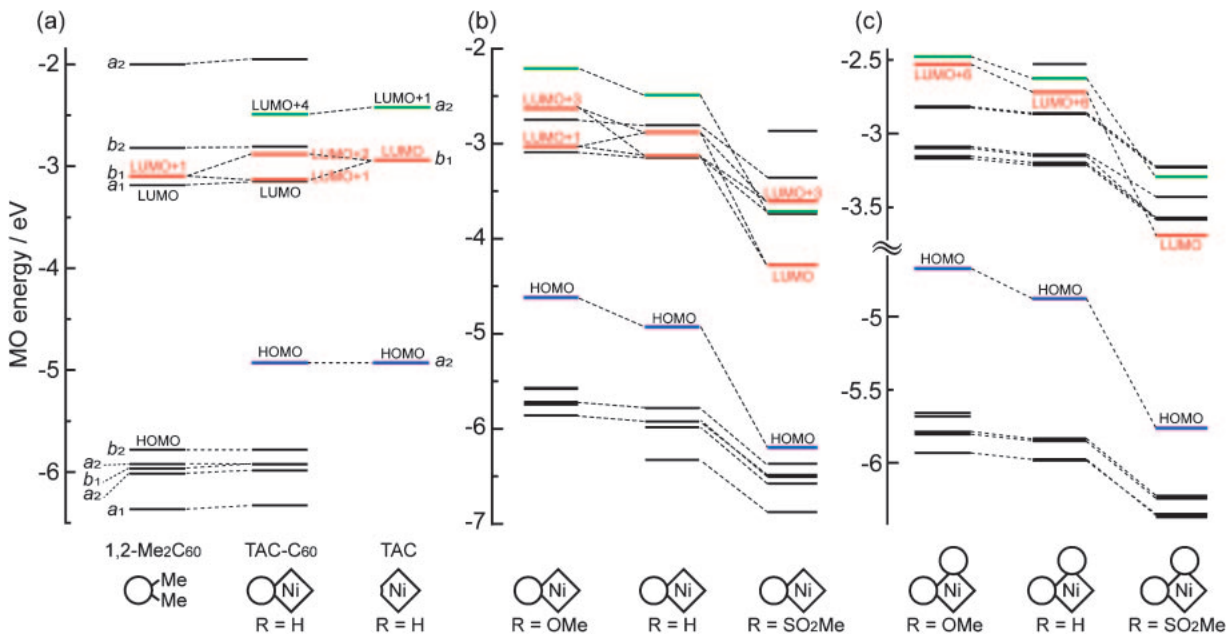

Figure 21. Partial MO energy diagram of (a) 1,2-$C_{60}Me_2$ (left), unsubstituted TAC–C_{60} (middle), and C_{60}-free TAC (right); (b) TAC–C_{60} with R = OMe (left), unsubstituted TAC–C_{60} (middle), and TAC–C_{60} with R = SO_2Me (right); and (c) TAiB–C_{60} with R = OMe (left), unsubstituted TAiB–C_{60} (middle), and TAiB–C_{60} with R = SO_2Me (right). For TAC–C_{60} (**49** and **50**) and TAiB–C_{60} structures (**51** and **52**), see Scheme 5.

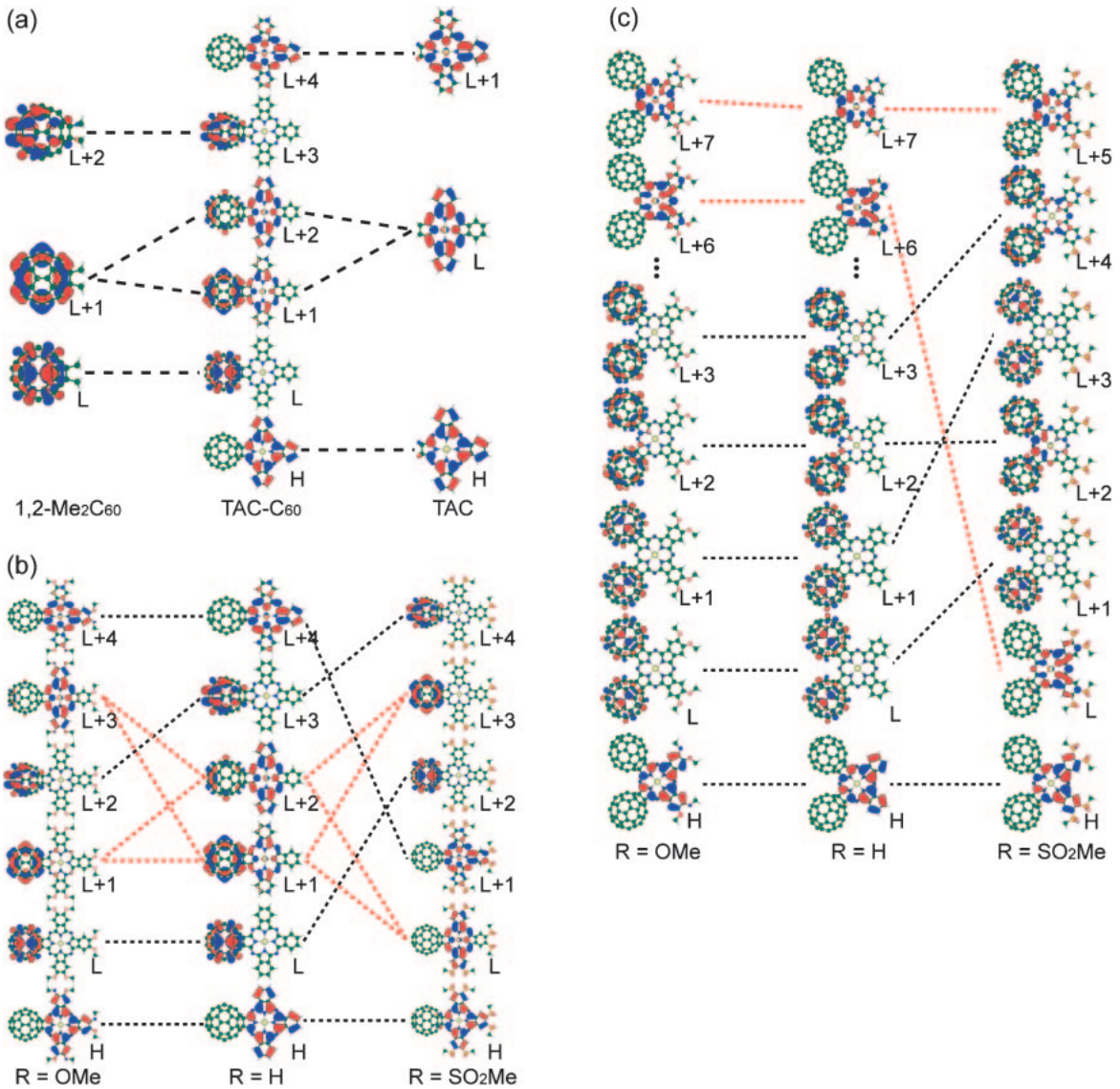

Figure 22. MOs which are principally associated with the Q band of the systems appearing in Figure 21. The HOMO and LUMO are represented as H and L, respectively.

types of deformations, called saddle and ruffle types, are known. In the former case, two pyrrole rings at opposite sites are displaced from a mean plane (typically the 4N(pyrrole)-plane) upwards, and the other two opposite pyrrole rings are displaced downwards, while the *meso*-carbons are not significantly displaced. In the latter case, however, the *meso*-carbons are displaced alternately up and down, and as a result β-carbon atoms at diagonal positions are displaced in the same direction from the 4N-plane. In contrast, metallophthalocyanines (MPcs) and metallotetraazaporphyrins are generally quite flat. For example, the average deformation of the Ni atom of NiPc from the average plane consisting of four pyrrole nitrogens is known to be less than 0.06 Å.[43b] Accordingly, research on deformed Pcs only began in the 21st century. When eight phenyl groups were introduced onto the benzene periphery closest to the Pc core, the Pc plane deformed to a saddle-type structure, where the adjacent pyrrole rings deviate up and down alternatively (Figure 23). Moreover, the extent of this deviation was the largest reported to date, even including normal porphyrins.[45]

Figure 23. X-ray structure of saddle type **60**.[44]

Following this result, the relationship between the extent of deformation and the spectroscopic or electrochemical properties was examined by controlling the number of introduced

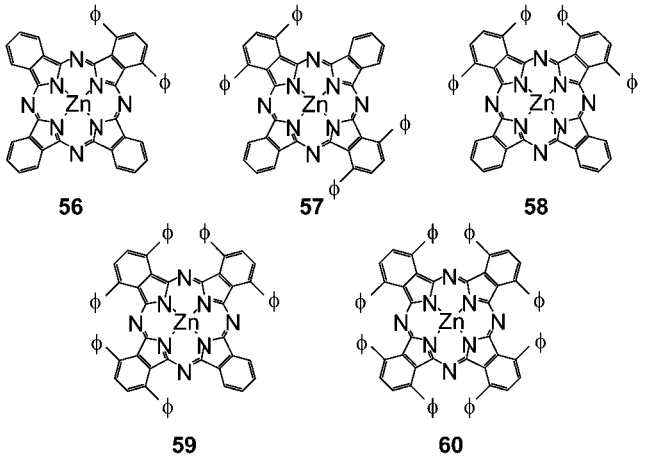

Scheme 6. Structures of phenylated (deformed) zinc phthalocyanines.

phenyl groups.[44] Thus, 2, 4, 6, and 8 phenyl groups were introduced, and the extent of deformation examined by X-ray spectroscopy (compounds **56**–**60**, Scheme 6). Deformation was observed only when phenyl groups were introduced onto adjacent benzene rings of Pcs. Although the spectrum changes on introduction of substituents groups, the change by this effect was estimated from the data of Pc compounds without deformation, i.e., from the data of Pcs without substituent groups, and those with two phenyl groups in one benzene ring, **56**, and four phenyl groups at two benzene rings at opposite positions, **57**. With increasing deformation of the Pc core, the Q absorption band did shift to longer wavelength, more than for normal substituent groups. This effect was proportional to the increasing number of substituent groups. Utilizing this characteristic, the Q band of highly deformed Pcs can be shifted beyond 800 nm, which is the region of naphthalocyanine (Nc).[46] Electrochemical data were also consistent with the extent of the deformation, where the potential difference between the first oxidation and reduction became smaller than would be expected for normal Pcs without deformation (Figure 24). Ruffled type deformation is not known for Pcs to date.

A spectroscopically very interesting example of ring deformation was reported for low-spin divalent FePcs.[47] The iron ion was chosen since many charge-transfer transitions are predicted in addition to π–π^* transitions.

General D_{4h} Fe^{II} low-spin Pcs do not show absorption bands beyond the Q band, while the corresponding saddle-type D_{2d} Fe^{II}Pc (iron complex of **60**) showed two absorption peaks beyond the Q band. This was interpreted by suggesting that two charge-transfer transitions with forbidden character buried in the Q and Soret bands of D_{4h} FePc become allowed in D_{2d} symmetry and shift to the near-IR region. The MCD data revealed that one of these is a transition to a degenerate excited state, while the other is to a non-degenerate excited state, which is also consistent with group theory considerations.

This appearance of the Q band at longer wavelength opened the route to red Pcs,[48] while general Pcs are used as either blue or green dyes and pigments. The discovery of red Pcs has long been a target in Pc chemistry, since stable red dyes and

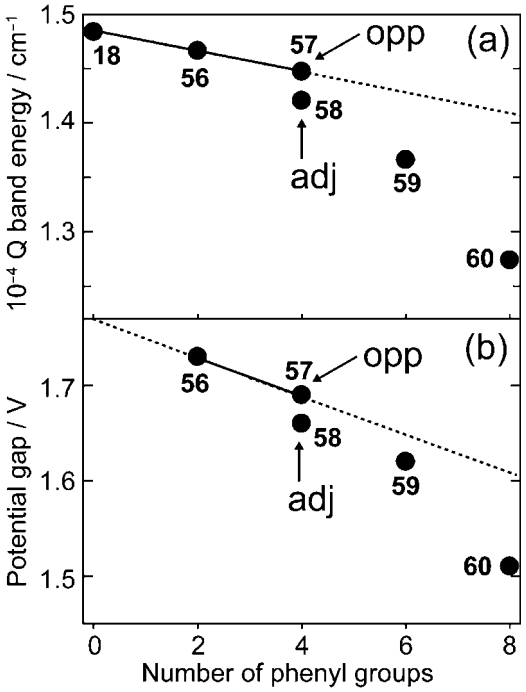

Figure 24. Relationship between deformation, Q band position and potential difference between the first-oxidation and -reduction potentials.

pigments do not exist and Pcs are stubborn compounds. The realization of red Pcs is due to two facts: the Q band is shifted to the near-IR region that we cannot see, while a new band appears at a longer wavelength of the Soret band in the red region at around 540 nm. Simultaneously, by selecting central metals, yellow and orange Pcs also become available. Similarly, red Pcs were realized by introducing eight alkoxy groups at the so-called α positions (Pc periphery closest to the Pc core) and selecting Mn as a central metal.[49] According to the data published so far,[50] all Pcs substituted by eight bulky or long electron-donating groups at the α positions deform to a saddle-type D_{2d} symmetry as a result of the steric hindrance between adjacent substituent groups which protrude up and down from the Pc plane.

5. Optically Active Phthalocyanine and Porphyrin Systems

Many researchers have reported optically active porphyrin and Pc systems to date.[51,52] However, even if the CD spectra of their compounds were reported, interpretation of the spectra was rarely performed, due perhaps to the difficulty of the theory for general organic chemists and biochemists. On the other hand, researchers who are proficient in theory could not present systems suitable for analysis, since they are generally less competent at preparing these types of system. In 1999, we reported an exemplary Pc system in order to show the beauty and effectiveness of CD spectroscopy,[53] where optically active binaphthyl units were linked to the Pc periphery. The relative intensity of the Soret vs. Q band, sign and shape of the CD spectra were all beautifully rationalized on the basis of CD theory. It was established that positive and negative CD sign is induced in the presence of left- and right-handed conformers. Therefore, for example, if the CD spectra of naturally occurring

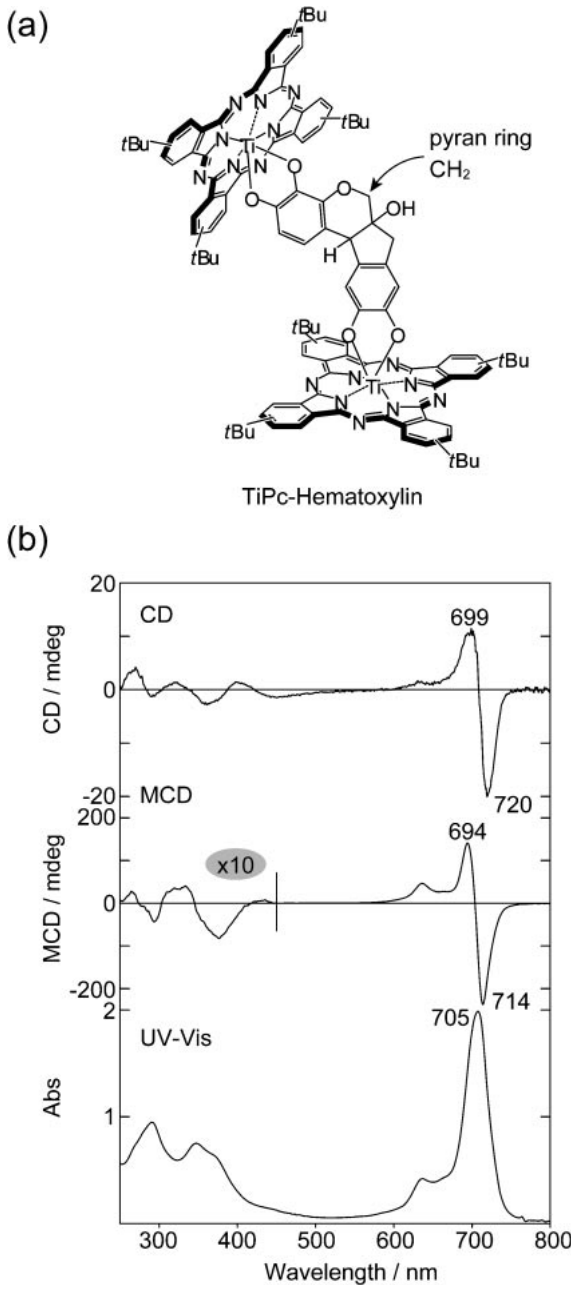

Figure 25. (a) Chemical structure of TiPc-linked hematoxylin complex and its (b) electronic absorption, CD, and MCD spectra in dichloromethane.

chlorophylls or hemoproteins show positive sign, the overall symmetry of the surroundings is judged to be left-handed.

In order to show the usefulness of CD spectroscopy, in 2004, the absolute configuration of hematoxylin was determined by analyzing the spectra of TiPc-linked hematoxylin (natural ortho diol type chiral compounds extracted from plants) (Figure 25), where its three-dimensional structure was analyzed by analyzing the excitonic interaction of two Pc-chromophores. This was possible since hematoxylin contains a plurality of catechol units and TiOPc was found to react with catechol to form a catechol coordinated (as an axial ligand) Pc.[54] With respect to the chemical structure of hematoxylin, it was known beforehand from NMR spectroscopy that it takes a cis type

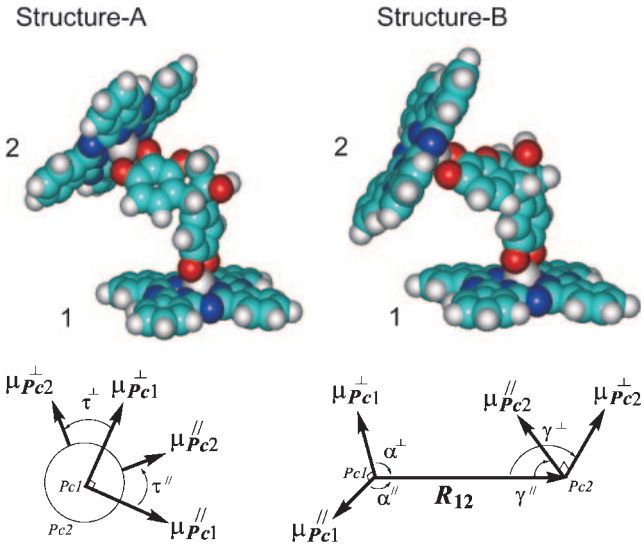

Figure 26. (top) Two possible low-energy conformers of TiPc–(6a*S*,11b*R*)-hematoxylin obtained from DFT calculations. Viewing from Pc1 to Pc2, it is left- and right-handed for structures A and B, respectively. (bottom) Geometrical parameters for CD analysis.

Table 2. Geometrical Parameters for the TiPc–(6a*S*,11b*R*)-Hematoxylin Complex (Figure 25a)

Structure		α	β	γ	R_{12}/Å
A	$\mu_{Pc}^{\parallel}$	81.96	84.20	40.03	13.20
	$\mu_{Pc}^{\perp}$	61.00	65.20	38.23	13.20
B	$\mu_{Pc}^{\parallel}$	62.75	90.01	351.70	13.01
	$\mu_{Pc}^{\perp}$	66.97	61.17	339.00	13.01

structure.[55] Of the conceivable absolute structure [(6aS,11bR) form], the two structures shown in Figure 26 (top) are possible, depending on the orientation of the CH_2-carbon of the pyran ring in the central moiety of hematoxylin (the structures to the left and right are distinguished as A- and B-structure, respectively). If we further discriminate the two Pc units by numbers 1 and 2, as shown in Figure 26 (top), and view the A- and B-structure from the Pc1 side to the Pc2 side, it will be left-handed and right-handed, respectively. Since the energy difference between the A- and B-structure is so small, the experimental CD spectrum was analyzed assuming that it was produced as a 1:1 mixture of structures A and B. Figure 26 (bottom) shows the electronic dipole moments ($\boldsymbol{\mu}$) on the Pc plane. $\parallel$ and $\perp$ denotes whether $\boldsymbol{\mu}$ is parallel or perpendicular, respectively, to the catechol plane linked to Ti. The presence of transitions with different polarization in the Q band region can be substantiated by the MCD signal of different sign. Although dipole–dipole approximation was used for the analysis, this was appropriate since the estimated TiPc–TiPc distance (ca. 13 Å) was much larger than the experimentally obtained length of $\boldsymbol{\mu}$ (0.8–0.9 Å). Within this approximation, the exciton energy ($\boldsymbol{\varepsilon}$) and rotational strength (i.e., CD intensity $\boldsymbol{R}$) of the degenerate coupled oscillator system can be expressed using four equations (eqs 1–4)[56] and adopting angles obtained from Figure 26 (top) (Table 2).

Table 3. Results of Coupled Oscillator Analysis for TiPc–(6a*S*,11b*R*)-Hematoxylin and Gaussian Fit Analysis of the Observed CD Spectrum for TiPc–Hematoxylin

		Energy /cm^{-1}	Wavelength /nm	Oscillator strength	Rotatory strength /$D\mu_b$
Structure A	$e^{\parallel}(-)$	14078	710.3	0.0337	−3.844
	$e^{\parallel}(+)$	14149	706.7	0.2358	3.844
	$e^{\perp}(-)$	14299	699.3	0.0653	−2.630
	$e^{\perp}(+)$	14378	695.5	0.1600	2.630
Structure B	$e^{\parallel}(-)$	14075	710.5	0.0156	0.783
	$e^{\parallel}(+)$	14153	706.5	0.2439	−0.783
	$e^{\perp}(-)$	14295	699.5	0.0491	1.547
	$e^{\perp}(+)$	14382	695.3	0.1762	−1.547
Gaussian fit		13954	716.7	0.0927	−0.935
		14245	702.0	0.7750	0.746

$$R^{\perp}(\pm) = \pm[\{\varepsilon_{Pc}{}^{\perp}(\mu_{Pc}{}^{\perp})^2 R_{12}\}/(4\hbar)] \sin\alpha^{\perp} \sin\gamma^{\perp} \sin\tau^{\perp} \quad (1)$$

$$\varepsilon^{\perp}(\pm) = \varepsilon_{Pc}{}^{\perp} \pm [(\mu_{Pc}{}^{\perp})^2/4\pi\varepsilon_0(R_{12})^3](\sin\alpha^{\perp} \sin\gamma^{\perp} \cos\tau^{\perp} + 2\cos\alpha^{\perp} \cos\gamma^{\perp}) \quad (2)$$

$$R^{\parallel}(\pm) = \pm[\{\varepsilon_{Pc}{}^{\parallel}(\mu_{Pc}{}^{\parallel})^2 R_{12}\}/(4\hbar)] \sin\alpha^{\parallel} \sin\gamma^{\parallel} \sin\tau^{\parallel} \quad (3)$$

$$\varepsilon^{\parallel}(\pm) = \varepsilon_{Pc}{}^{\parallel} \pm [(\mu_{Pc}{}^{\parallel})^2/4\pi\varepsilon_0(R_{12})^3](\sin\alpha^{\parallel} \sin\gamma^{\parallel} \cos\tau^{\parallel} + 2\cos\alpha^{\parallel} \cos\gamma^{\parallel}) \quad (4)$$

The results are summarized in Table 3 and shown as graphs in Figure 27a. As seen in this Figure, associated with the Q band, the CD sign sequence is different between the structures A and B. Figure 27b is the spectra obtained by adding the CD spectra in Figure 27a at a 1:1 ratio, together with the experimental spectra. Since the experimental sign sequence and intensity are reproduced, the absolute configuration of hematoxylin was determined to be (6aS,11bR) form.

A similar analysis was applied to apple procyanidines (Figure 28).[57] Procyanidins (condensed tannins) are a class of polymeric polyphenols which can be isolated from plants, and are responsible for the bitter, astringent taste of certain beverages and foodstuffs as well as their color, flavor, and longevity. The CD spectra of dimers, trimers, and tetramers of polycyanidins were analyzed by linking TiOPc at their catechol units, and it was concluded that the helicity is left-handed on the basis of the CD analyses.

Two porphyrins linked by short alkyl group **61** can be optically active if the two porphyrin units can make single-handed rotation as viewed from one side. Figure 29 shows an example of this type of phenomenon.[58] Two zinc porphyrins can be arranged in either right- or left-handed rotation by the addition of optically active diamines, since amine coordinates to two zinc ions and fixes the molecular structure. The experimental spectra are shown in Figure 29b (left). Corresponding to the absorption maxima, troughs and peaks are observed in both the CD and MCD spectra. MCD is sensitive for transitions in one chromophore unit; however, since there is no degenerate excited state in the system shown in Figure 29a, all transitions appeared as Faraday *B*-terms of Gaussian shape. An important result from the MCD spectrum is that the two transitions at 410 and 419 nm are indeed of different polarization (note that the CD sign is positive in this region). The

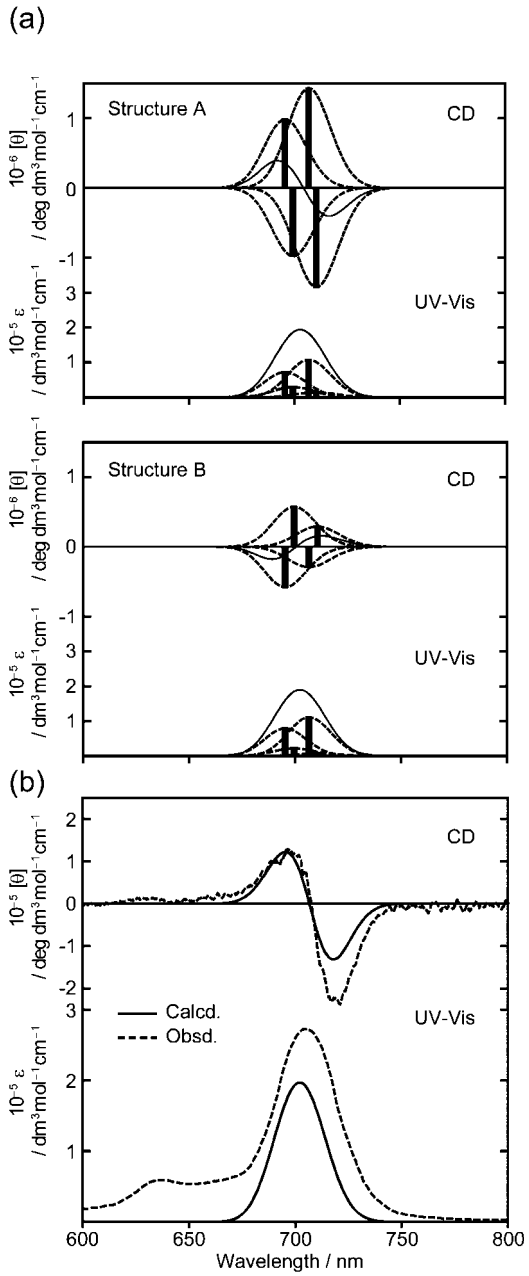

Figure 27. (a) Calculated electronic absorption and CD spectra of the two conformers in the TiPc–(6a*S*,11b*R*)-hematoxylin complex. Each band was described by a single Gaussian curve (broken lines). The solid lines indicate the superposition of all Gaussian curves. (b) Comparison between the experimental spectra of TiPc–hematoxylin and the calculated spectra generated by superimposing the spectra of the two conformers for a (6aS,11bR) form 1:1 mixture.

theoretical CD spectrum of this system was calculated using its X-ray structure (Figure 29b (right)). In each porphyrin, there are two transitions which have parallel ($B_{\parallel}$) and perpendicular ($B_{\perp}$) orientations to the ethano-bridge, and these result in two major types of degenerate exciton interaction ($B_{\parallel}$–$B_{\parallel}$ and $B_{\perp}$–$B_{\perp}$couplings), thus leading to four exciton states (Figure 29b (right)). As can be seen in Figure 30, the relative

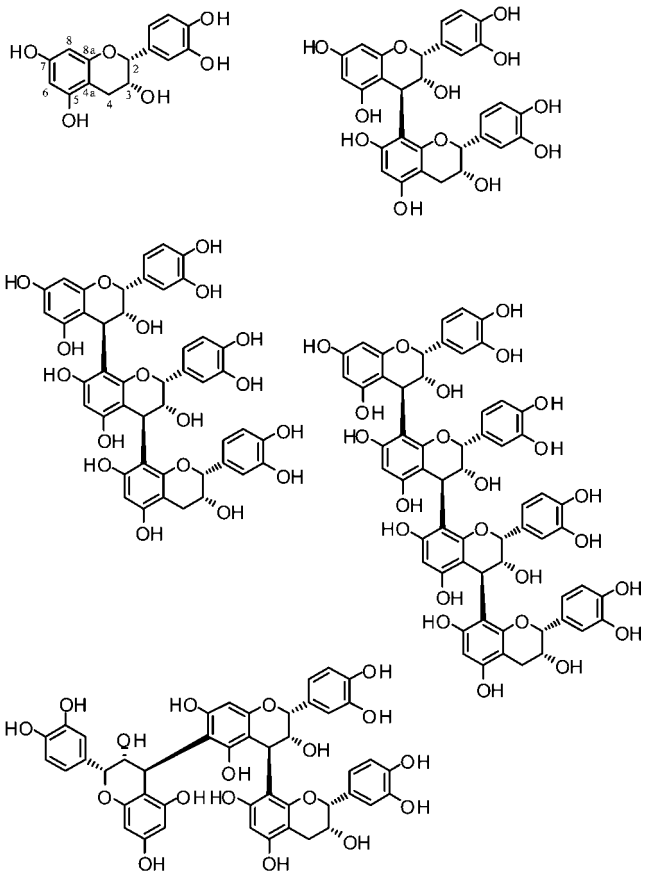

Figure 28. Structures of some representative procyanidins.

orientation between these two pairs of electronic transition is anticlockwise, which according to the excition chirality method,[59] predicts the negative chirality that was observed experimentally (minus to plus in ascending energy).

More than a quarter century ago, a porphyrin-appended cyclodextrin (CDx) **62** was prepared (Figure 31).[60] Since porphyrins are too large to be accommodated into the cavity of CDxs as chiral-inducers, while CDxs can trap small molecules, we felt that guest-induced conformational changes might be seen in the CD spectra of compounds like **62**. In water, **62** shows a spectrum typical of aggregated porhyrins. When a guest is trapped in the cavity of CDx, it experiences multiconformational (five-step six-stage) changes over a period of 21 h (Figure 31), which was confirmed by circular dichroism changes accompanying a set of isoelliptic points. Since this phenomenon was always observed when the guest concentration attained a certain value, it was concluded that the effect is a guest-induced multiconformational change.

Porphyrin dimers sharing a common aromatic ring cannot be analyzed by exciton coupling theory[59] since there is conjugation to some extent through the common ring. This type of porphyrin **63** (Figure 32) was analyzed using electronic absorption, MCD, and CD spectroscopies, together with MO calculations. Indeed, the reason we analyzed **63** was that we found an incorrect analysis (and therefore wrong conclusion!) of this compound.[61b] Using X-ray structural data, calculations revealed (Figure 33) that the dimer has a right-handed structure, which is just the opposite conjectured from exciton

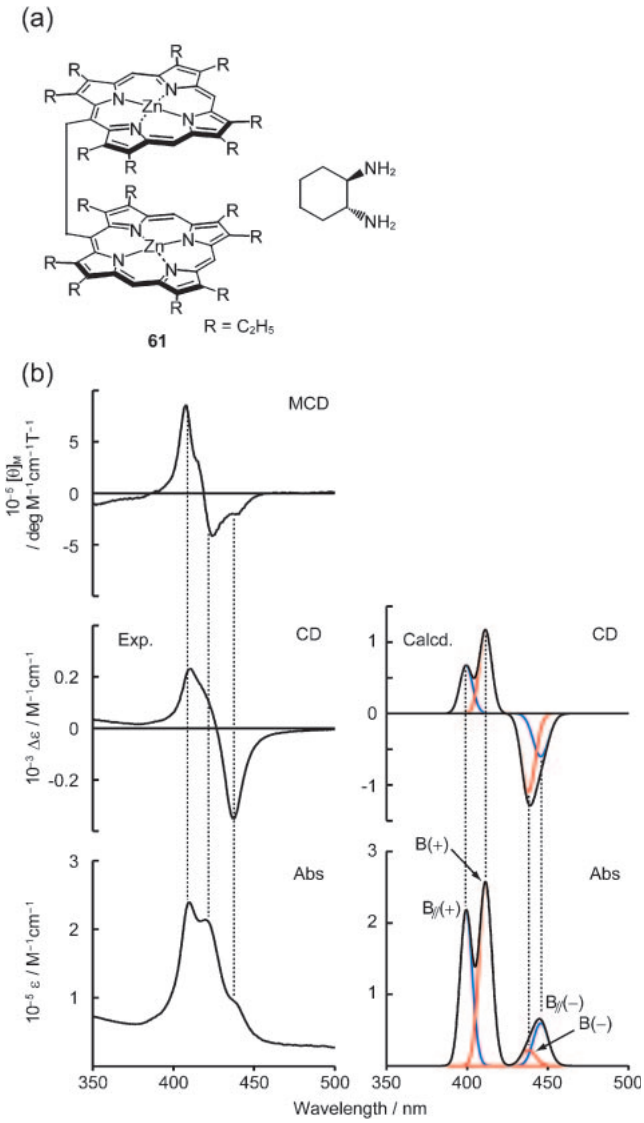

Figure 29. (a) Chemical structures of bis(zinc octaethylporphyrin) **61** and (*R*,*R*)-diaminocyclohexane. (b) Experimental MCD, CD, and absorption spectra recorded in dichloromethane (left), as well as the calculated CD and absorption spectra (right) of the Soret band region. Each calculated exciton band was described by a single Gaussian curve. The notations plus and minus represent the in-phase and out-of-phase transitions, respectively.

coupling theory. Although exciton coupling theory is often used by organic chemists, this theory should not be used for conjugated systems, since in the exciton theory, the interaction of independent chromophoric groups is postulated.

The validity of using vibrational CD spectroscopy for porphyrinoids has not yet been reported. Accordingly, in order to examine the validity, the vibrational CD spectra of several optically active porphyrazine complexes have been recorded,[39] and it was found that vibrational CD is effective for compounds containing optically active aliphatic rings (for optically active compounds consisting of only aromatic groups, this spectroscopy was found to be of little use). Since the CD calculations predict the experimental data so nicely in both

energy and intensity, it is now possible to determine the configuration of aliphatic compounds by utilizing this spectroscopy.

6. Definitive Assignment of Absorption Bands of Planar and Sandwich Type Porphyrinoids by MCD Spectroscopy

The spectroscopic assignments of the absorption bands of sandwich and planar porphyrinoids have often been discussed by several researchers.[62a] However, the assignments were not necessarily consistent because of the large π systems, which render molecular orbital calculations difficult, and due to the lack of systematic work. The assignment must match the experimental data and if possible be explained conceptually. Osuka et al. reported a series of planar porphyrin oligomers **64**–**67** connected at pyrrole β–β, *meso*–*meso* carbon, and other pyrrole β–β positions (Figure 34) and their absorption spectra in CH_2Cl_2. Thereafter, a route for assigning the absorption spectra of the dimer **65** by MO calculations was also published.[62b] However, since the spectra had a strange shape in the bands at the longest wavelengths, we decided to remeasure the absorption and MCD spectra in pyridine, where aggregation behavior appears depressed by coordination of pyridine to the central metals. The shape and position of the band at longest wavelength (Q band) was altered dramatically by changing the solvent from CH_2Cl_2 to pyridine, and the shape in pyridine appeared similar to that of normal porphyrins (Figure 34), although the change in the Soret region was marginal. Although it was easily conjectured from the D_{2h} symmetry of the oligomers that the Q band splits into two, the position of the second component was unclear in the absorption spectra (the first component was an intense band at the longest wavelength). By measuring the MCD spectra, however, the position was unambiguously determined as a tiny shoulder at the long-wavelength edge of the Soret band. That is, we used the MCD characteristic that interacting transitions produce an

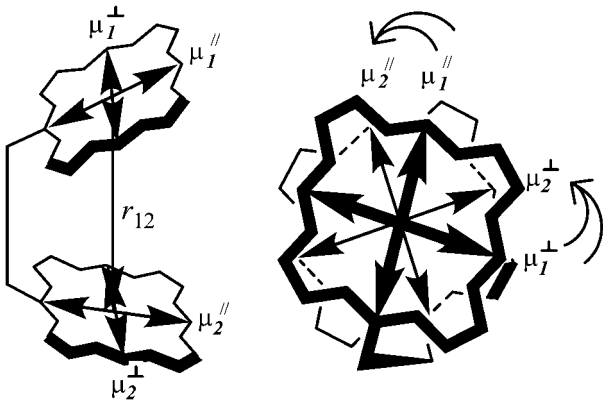

Figure 30. Definition of the direction of the transition dipole moments used in the theoretical analysis. r_{12} is the distance between the centers of gravity of the porphyrin units.

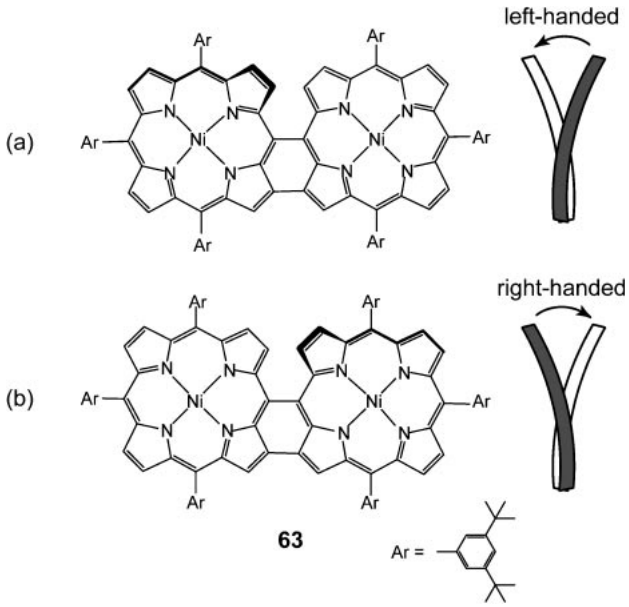

Figure 32. A planar porphyrin dimer sharing a common aromatic ring **63**.

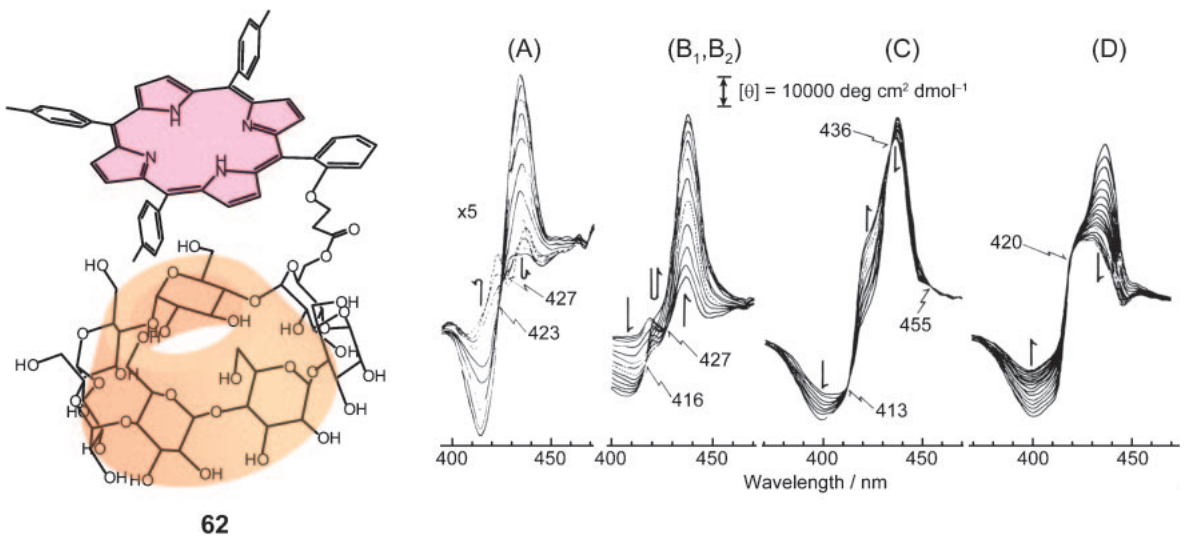

Figure 31. Porphyrin-appended CDx system, **62**, and its guest-induced multiconformational change, detected by CD spectroscopy. More than 20 h are required for the whole process to occur.

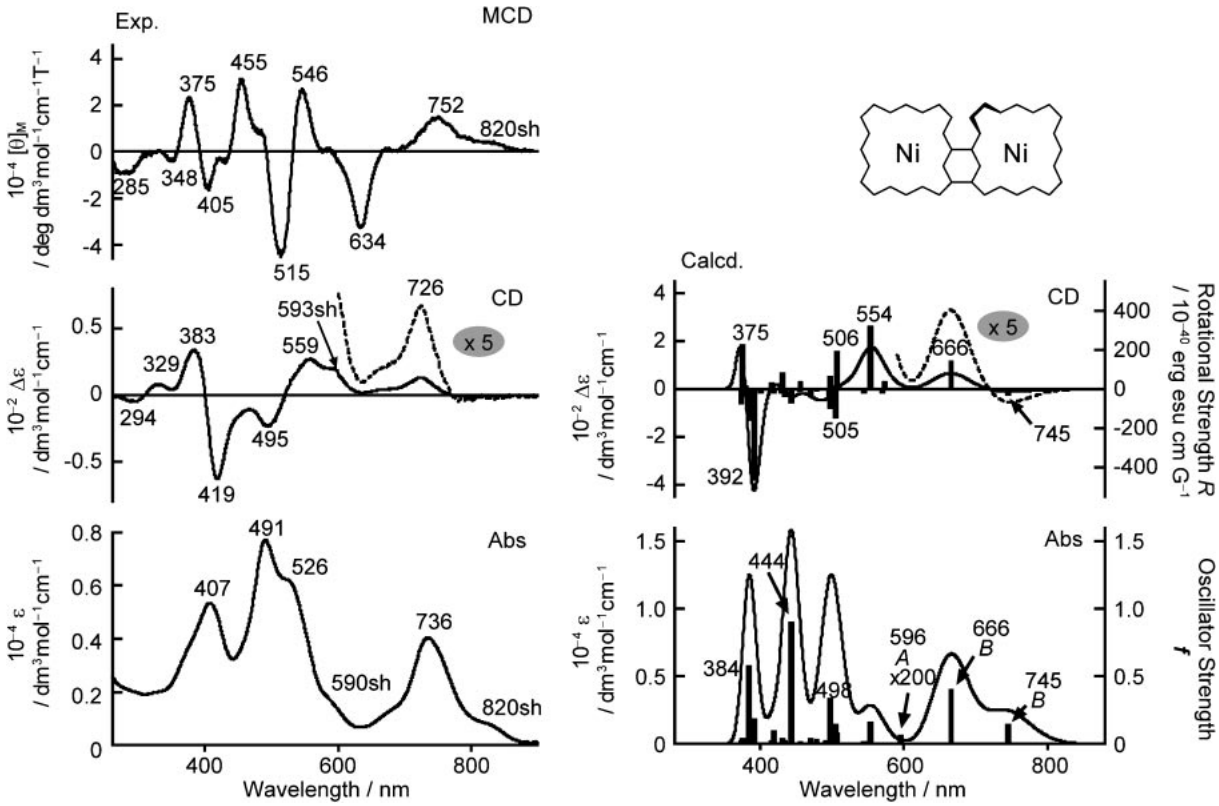

Figure 33. Experimental electronic absorption, MCD, and CD spectra of a porphyrin dimer **63** (left), and its calculated absorption and CD spectra (right).

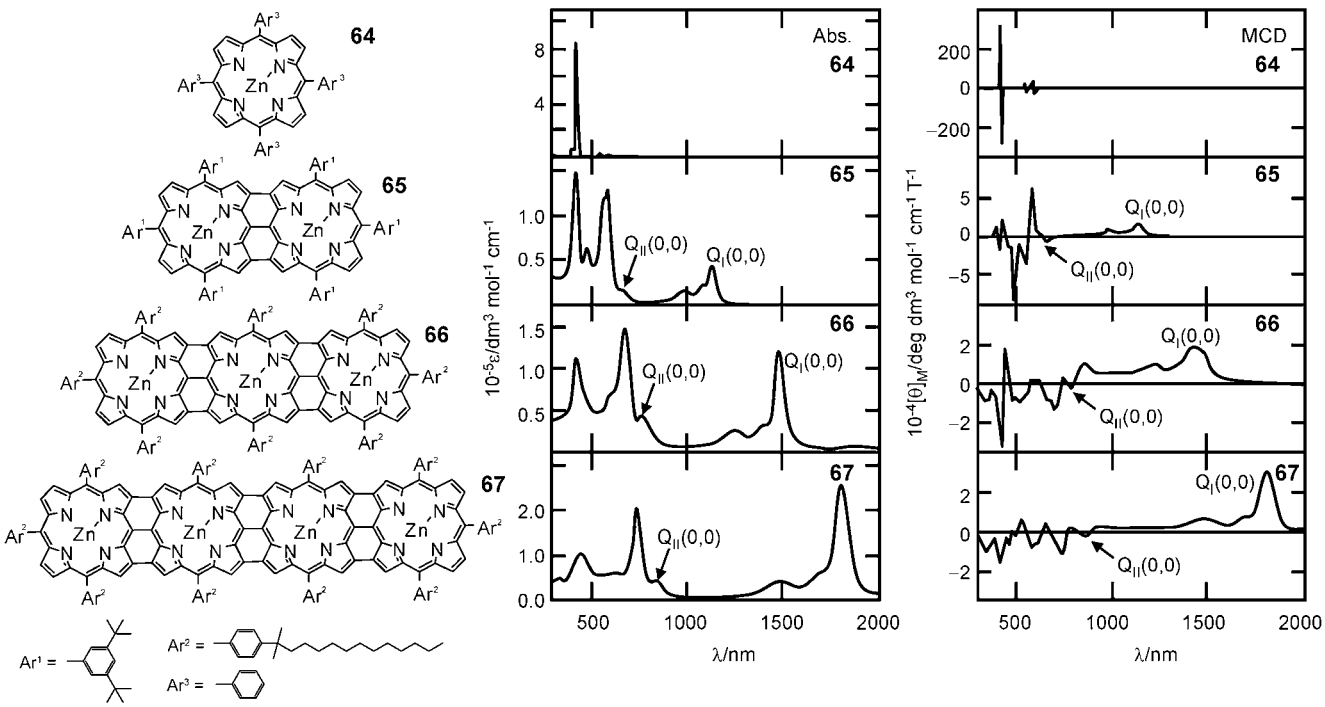

Figure 34. Structures of triply linked planar zinc porphyrin oligomers, and their absorption and MCD spectra in pyridine.

MCD sign of opposite sign.[63] Since the MCD sign for the band at the longest wavelength was positive, the sign for this tiny shoulder was negative for all oligomers. Furthermore, from this MCD pattern (plus-to-minus in ascending energy), it was suggested that ΔLUMO (the energy difference between the LUMO and LUMO+1) is larger than ΔHOMO (the energy difference between the HOMO and HOMO−1), and this was indeed reproduced by MO calculations.[64] In Ref. 62b, this

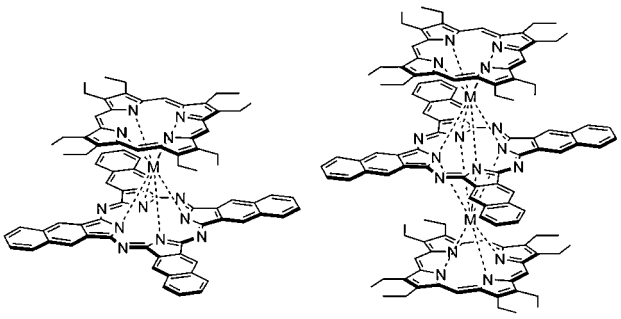

Figure 35. Examples of chemical structures of OEP–Nc rare-earth double and triple sandwich complexes.

second component of the split Q band was not taken into consideration, and the vibrational band of the band at longest wavelength was mistakenly assigned as the split component, thus revealing the danger of assigning the absorption bands on the basis of only MO calculations.

Porphyrins and phthalocyanines can form homo- and heteroleptic sandwich dimers or trimers when reacted with rare-earth metal elements (Figure 35).[65] An important spectroscopic problem with these compounds is the assignment of their absorption bands, which has been a target of long debate.[62a] In the case of homoleptic dimers, the rotation angle between the two ligands depends on the ionic radius of the central metal: the smaller the radius, the larger the angle. Even if the central metal is changed, the produced spectrum remains similar, since only the ionic radius is changed slightly. When we reacted octaethylporphyrin (OEP) and naphthalocyanine (Nc) with rare-earth elements, we found fortunately in the X-ray data of the resultant eclipsed compounds that the rotation angle between the two ligands does not essentially depend on the central metal.[66] Accordingly, we were able to discuss the spectra only as a function of the distance between the two ligands. Figure 36 shows the absorption and MCD spectra of La **68** and Dy **69** complexes.[67] Corresponding to the absorption peaks designated by I, II, and III, a very small negative (hardly seen on this scale), differential, and differential type MCD peaks appeared. Peaks I and II shift to shorter and longer wavelength, respectively, accompanying a decrease in ionic radius. Constructing MOs of the complexes using constituent Nc and OEP (Figure 37), it is understood that the assignments I and II in this figure can clearly reasonably explain the shift of bands and MCD spectral pattern. Here, with decreasing metal ionic radius, band I shifts to shorter wavelength since the energy difference between the anti-bonding SOMO and bonding HOMO becomes large. In addition, the observed MCD signal is a Gaussian type Faraday *B* term since the SOMO is not degenerate. On the other hand, transitions corresponding to II shift to longer wavelength since the energy difference between the two orbitals decreases with decreasing ionic radius, and the corresponding MCD is a differential type Faraday *A* term as the excited state is doubly degenerate. These assignments were further confirmed by examining the spectra of singly-oxidized and reduced species: bands II and I

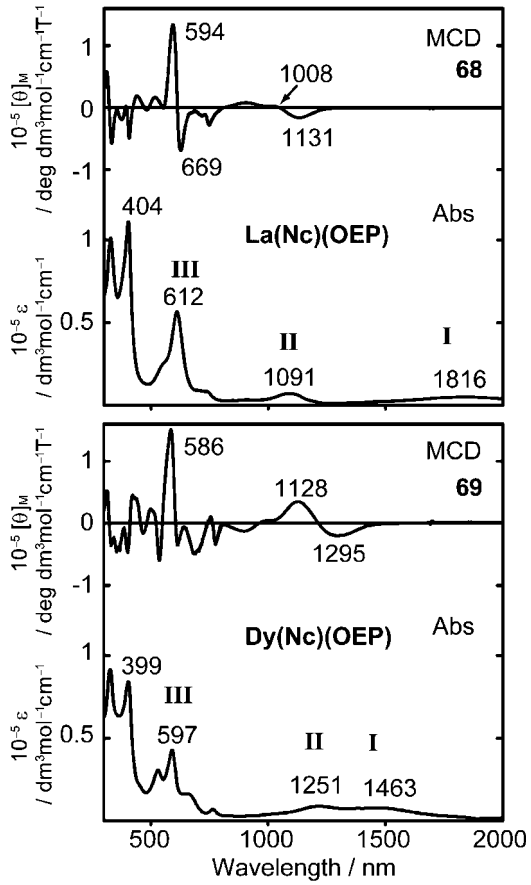

Figure 36. Electronic absorption and MCD spectra of La(Nc)(OEP) (**68**) and Dy(Nc)(OEP) (**69**) recorded in $CHCl_3$.

disappear in the oxidized and reduced species, respectively, since an electron is removed from the SOMO in the former case, while the SOMO is occupied by two electrons in the latter case.

Figure 38 shows the spectra of two triple decker complexes, **70** and **71**, and their assignments. MCD shows differential type Faraday *A* terms corresponding to all absorption peaks, indicating that the excited states are all degenerate (of course Faraday *B* term type MCD curves observed for the double deckers were not observed). Taking into account the change of redox potentials and spectral position on ionic radius, the bands I, II, and III were rationalized as indicated in the figure.

7. Other Porphyrinoid Work in Which Molecular Structures Play an Important Role

A hemiporphyrazine **72** prepared from two molecules each of isoindolediimine **73** and 3,5-diaminotriazole (**74**) has been known for many years, and exhibits an orange color.[68] Since replacement of the nitrogen by a sulfur atom generally results in compounds with a bathochromically shifted color, we had intended to obtain the corresponding compounds with a blood-red color. Thus, *t*-butylisoindolediimine **75** and 2,5-diamino-thiadiazole (**76**) were reacted (Scheme 7), but the resultant compound **77** was found to be composed of three molecules each of the starting two compounds.[69] Since the most obvious

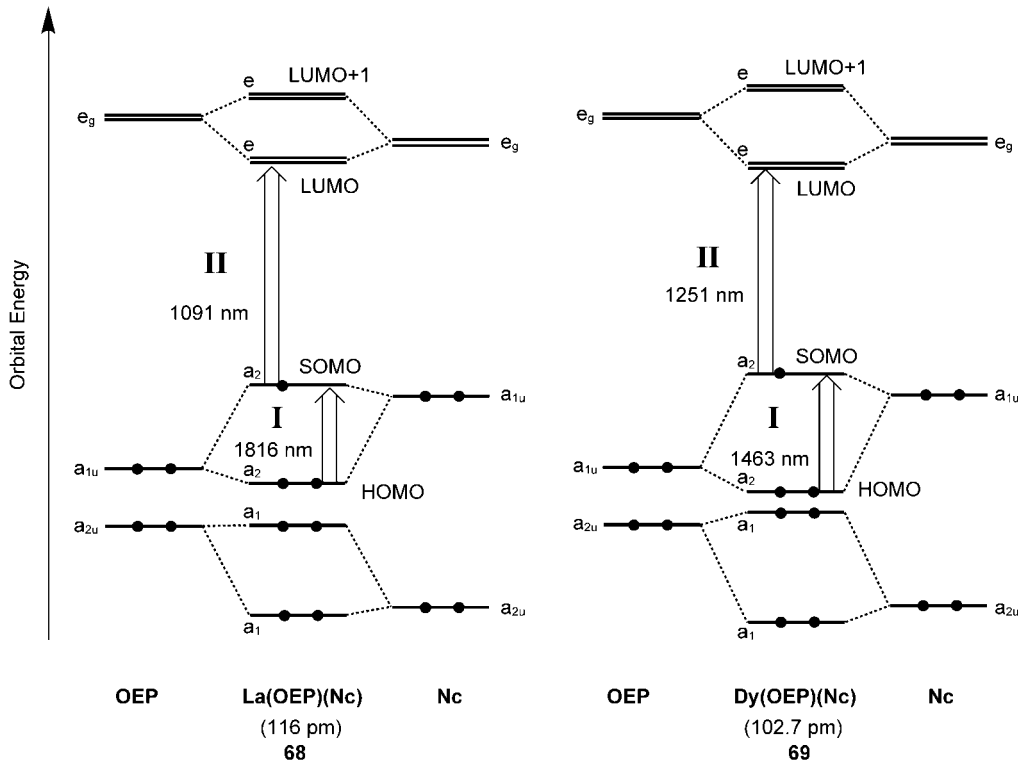

Figure 37. Schematic representation of the frontier MO energies for the C_{4v} sandwich dimer M(OEP)(Nc) with larger (M = La, **68**) and smaller (M = Dy, **69**) central metals. The value in the parentheses indicates the size of the central metal.

difference between 3,5-diaminotriazole (**74**) and 2,5-diaminothiadiazole (**76**) is the angle of NH_2–C–N–C–NH_2 (141°) and NH_2–C–S–C–NH_2 (164°), it was concluded that the wide angle of the latter made possible the formation of "3 + 3" type macrocycles. Interestingly, these "3 + 3" type compounds were found to trap three transition-metal ions such as Fe, Zn, Ni, and Co in close vicinity.[70]

The synthesis and solution properties of the so-called 15-crown-5-ed phthalocyanine was reported in 1987.[71] One of the most important properties is to trap cations such as K^+, Na^+, Ca^{2+}, and Cs^+ in the cavity of the crown moiety. Encapsulation of Ca^{2+} was examined using crowned CoPc **78** adsorbed on an Au electrode surface using scanning tunneling microscopy (STM).[72] We noticed first that the arrangement of the crowned Pc changes slightly after the addition of Ca^{2+} (this phenomenon is identified easily since a Co atom is very bright in the STM image), and also found that only two crown-ether moieties at diagonal positions become bright (Figure 39). After careful inspection, it was found that, at these positions, the hollow made by three gold atoms matches the center of the crown ether moiety. That is, Ca^{2+} can be trapped only in these hollows, and if the two crown ether units are fixed on the gold electrode surface, the centers of the other two crown ether units at diagonal positions do not match the hollow of the three gold atoms.

8. Optically Active Polymer Systems

Circular dichroism of naturally occurring optically active polymer systems has been examined by many researchers to date.[73] However, these systems are not necessarily good systems for showing the validity of CD spectroscopy. We analyzed the CD spectra of synthetic β-polypeptides **79** consisting of *p*-(optically active) alkylaminobenzoyl units in a main chain (Figure 40).[74] As seen in this figure, two absorption peaks appeared at ca. 300 and 260 nm, and the corresponding CD sign was positive and negative, respectively. What we had to do first was to assign the origin of these bands, and for this purpose, the spectra of β-cyclodextrin (β-CDx)–*p*-methylaminobenzoic acid complex were examined. β-CDx accommodates one *p*-methylaminobenzoic acid in its cavity as an axial inclusion (in this inclusion, the long axis of the guest matches the direction of the CDx axis). In such a case, it is already substantiated that transitions parallel to the CDx axis give a positive CD sign, while those perpendicular to the axis produce a negative CD sign.[75] In the present system, there are two absorption peaks at 305 and 227 nm, and the corresponding CD spectral envelope was plus and minus, respectively (Figure 41). Accordingly, it was found that the 300 and 260 nm bands in the polymer originate from the transitions along the long- and short-axis of *p*-methylaminobenzoic acid, respectively. Furthermore, taking into account the X-ray data for the trimer to hexamer showing that three residues make approximately one-turn, the transition to the lowest excited state becomes forbidden (in the case of the cyclic trimer, the sum of three vectors becomes zero), while that to the second excited state becomes allowed (Figure 42). However, in the case of the helix, the transition to the lowest excited state also becomes allowed, since the *z*-component of the transition dipole along the axis of the helix remains. Thus, the bands at ca. 300 and 260 nm in Figure 40 can be reasonably assigned. The next step was how to explain the CD sign. CD intensity, *R*, is expressed as $R = \mathrm{Im}(\boldsymbol{\mu} \cdot \boldsymbol{m})$ where $\boldsymbol{\mu}$ is the transition electric

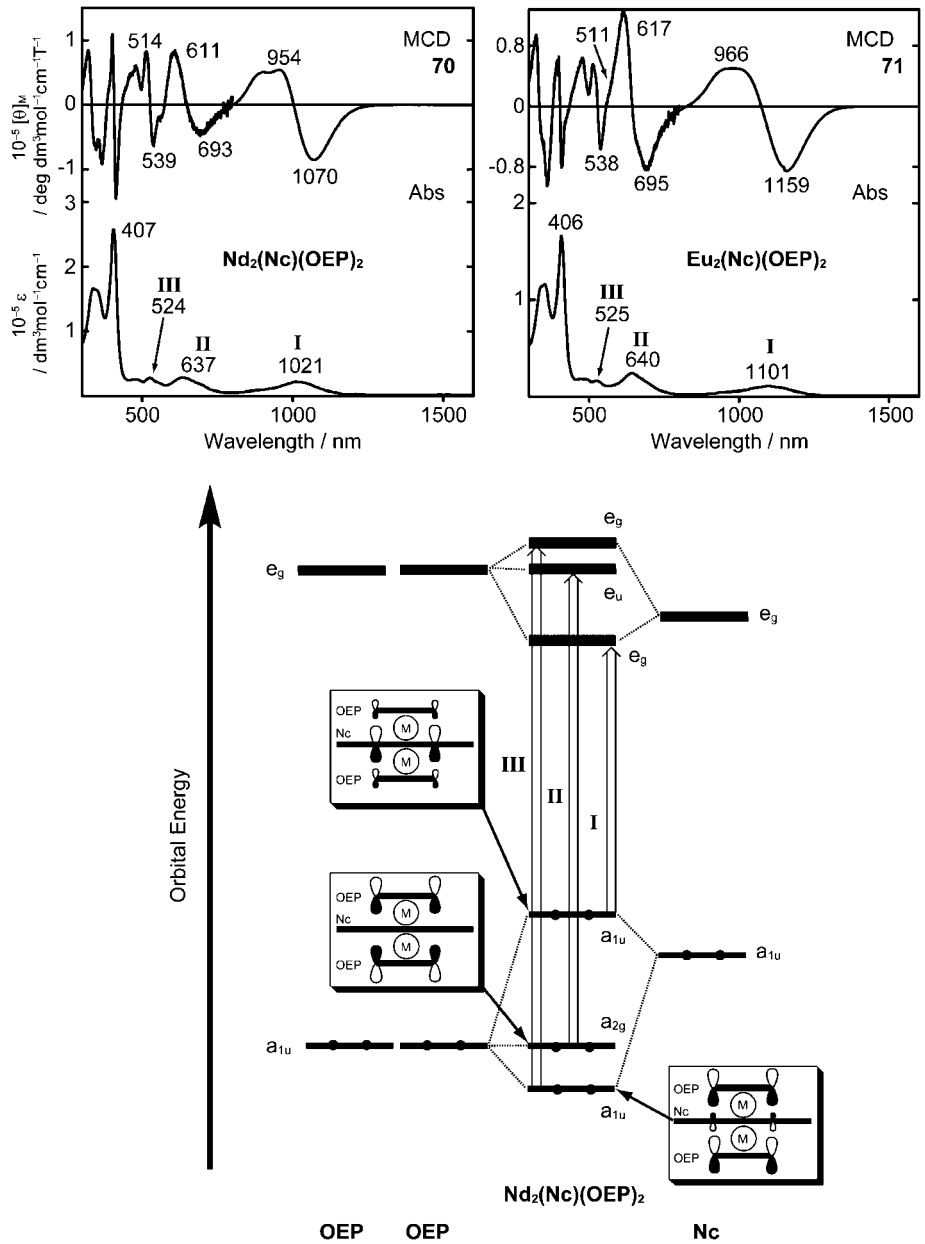

Figure 38. Electronic absorption and MCD spectra of $M_2(Nc)(OEP)_2$ (**70**: M = Nd and **71**: M = Eu) recorded in $CHCl_3$ (top). Schematic representation of the frontier MO energy levels of the D_{4h} triple-decker, $M_2(Nc)(OEP)_2$ (bottom).

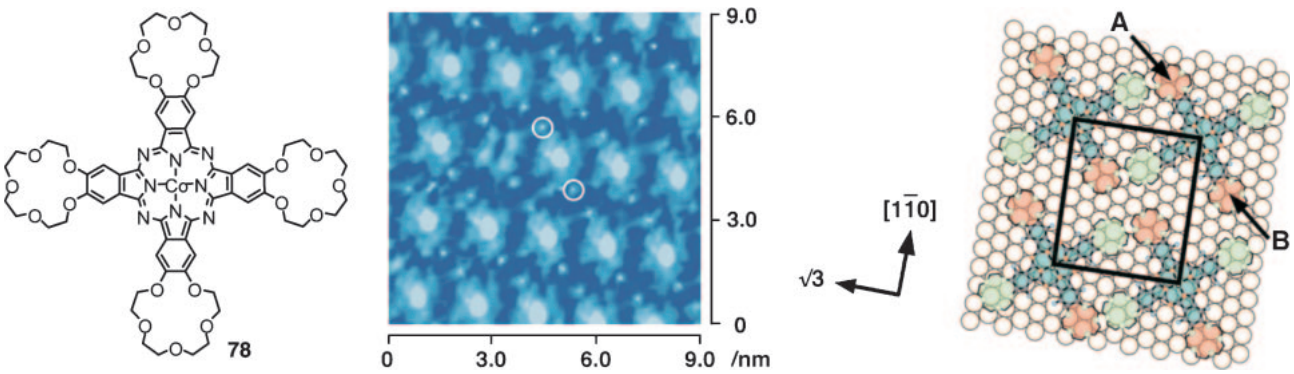

Figure 39. Crowned CoPc **78**, high-resolution STM images of **78** on an Au(111) surface in the presence of Ca^{2+} and model. In the model, the orange and green crown units represent complexed and uncomplexed units, respectively.

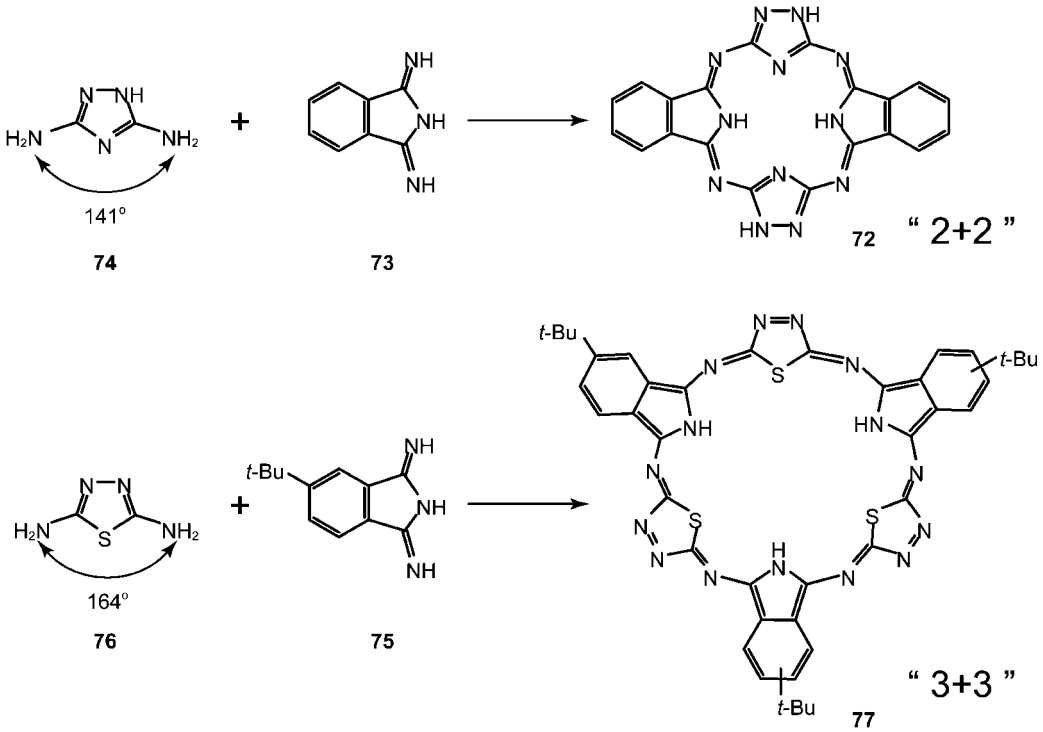

Scheme 7. Formation of hemiporphyrazines **72** and **77** from isoindolediimine **73** or **75** and 3,5-diaminotriazole (**74**) or 2,5-diaminothiadiazole (**76**).

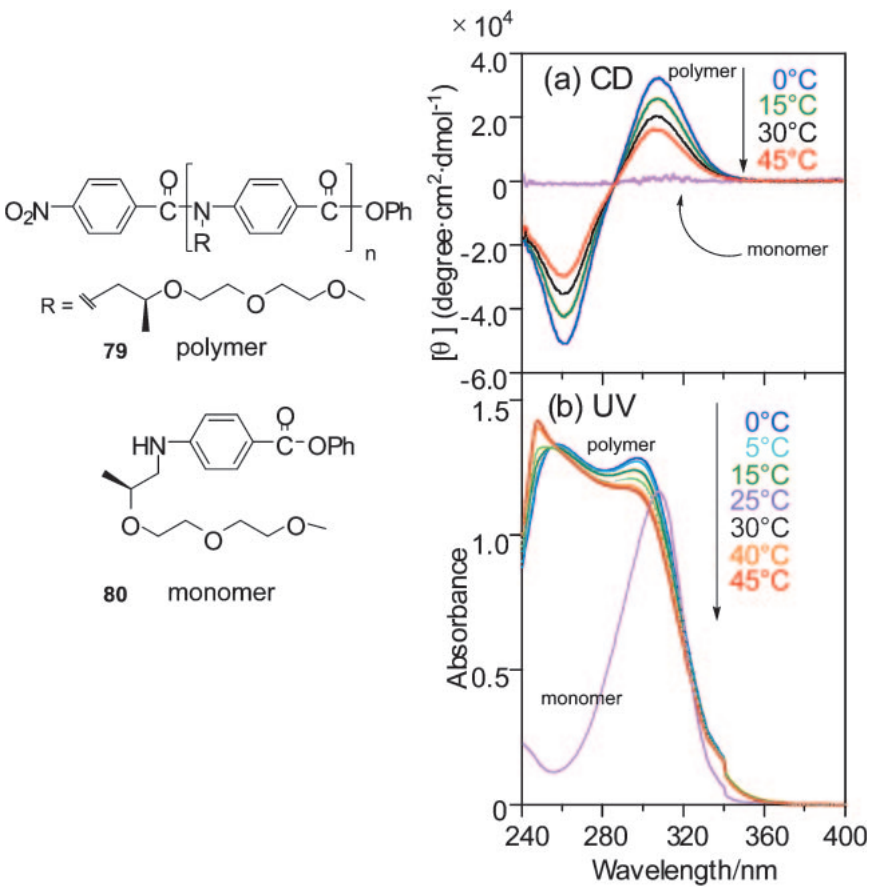

Figure 40. Chemical structures of optically active polymer **79** and the corresponding monomer **80** (left), and CD and electronic absorption spectra of **79** and **80** recorded in $CHCl_3$ (right).

dipole moment and ***m*** describes the transition magnetic dipole moment, which is related to the net circulation of electrons.[76] The equation implies that the sign of the CD is simply determined by the relative arrangement of ***μ*** and ***m***. In the case of the present polymers, the two coupling modes that give rise to the lower energy positive CD and the higher energy negative CD bands were associated with the net electronic transition moments that lie, respectively, parallel and perpendicular to the helix axis. Since the coupling between ***μ*** and ***m*** is described as a scalar product, what we had to do was to consider only these transition moments along the same axis for determining the origin of the optical activity.

Overviews of the direction of the net transition moments for a right-handed (P helix) and left-handed (M helix) helical

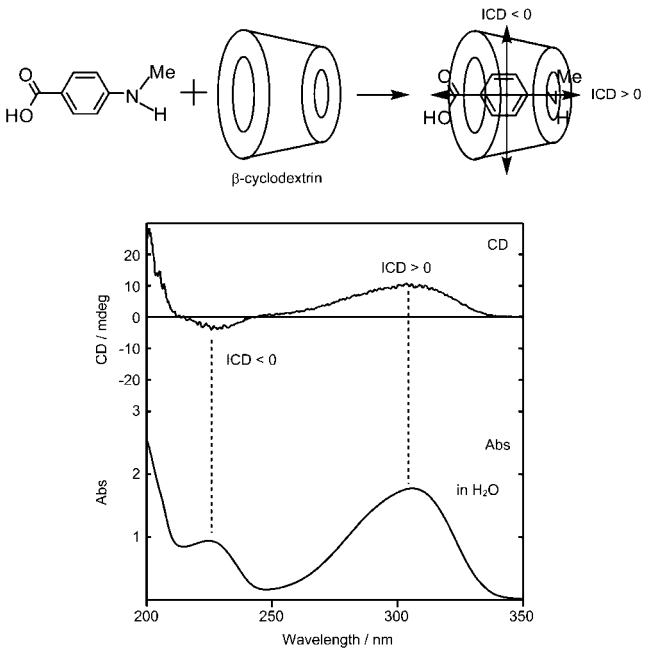

Figure 41. CD and electronic absorption spectra of *p*-methylaminobenzoic acid in water in the presence of *β*-CDx.

polymer with three light-absorbing units per turn are presented in Figure 43. It should be noted that the coupling of the transitions along the long axis induces the net transition magnetic dipole moments (***m***). The lower energy exciton state can be presented as head-to-tail couplings of neighboring transition moments, giving rise to ***m*** parallel or anti-parallel to the *z* axis because of the circulation of the transition electric moments (***μ***). On the other hand, the doubly degenerate higher exciton state has ***m*** directed along the *x*′ or *y* axis. By considering the scalar product of ***μ*** and ***m***, a theoretical CD pattern can be predicted. For example, in the case of the P helix, ***μ*** and ***m*** have the same sign along the *z* axis so that a positive CD is observed at a lower energy band, while they become opposite in sign along the *x*′ and *y* axes, which generate a negative CD at shorter wavelength. Of course in the case of the M helix, the opposite result is seen, where negative and positive CD signs (mirror image of that of the P helix) are predicted in ascending energy, and the positive and negative CD signals have the same intensity because of the sum rule.[59,76] Thus, in Figure 41, since the experimental CD spectra shows positive and negative CD signs corresponding to the absorption bands at ca. 300 and 260 nm, respectively, it could be concluded that N-alkylated poly(*p*-benzamide) preferentially takes a right-handed helical geometry.

The second example of a polymer is poly(isocyanide) containing optically active side chains.[77] Although optically active poly(isocyanide) shows a broad absorption band at ca. 300–460 nm, and either positive or negative CD bands in the same wavelength region, the relationship between the CD sign and helix sense was not elucidated except for a trial due to calculations.[78] In order to solve this problem, a block-copolymer of aryl isocyanide containing tetraphenylporphyrin and L-menthyl groups as pendant groups, **81**, was prepared, and its absorption and CD spectra analyzed (Figure 44) In addition to a broad absorption due to the poly(isocyanide) main chain, absorption due to the porphyrin is seen in the region of ca. 360–600 nm. The Soret absorption band is much broader than that without aggregation, indicating the presence of porphyrin–porphyrin chromophoric interaction. The CD spectrum of this

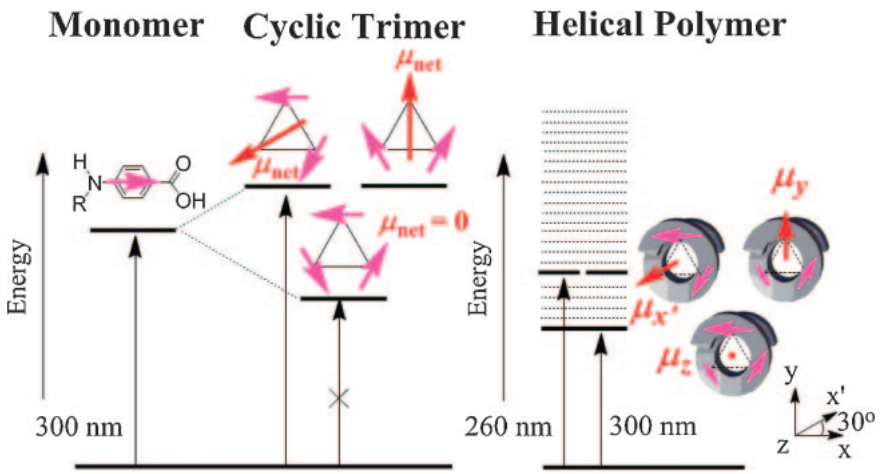

Figure 42. Schematic exciton band energy diagrams for a cyclic trimer and a helical polymer with three light-absorbing units per turn. The pink and red arrows indicate the transition electric dipole moments of each *p*-aminobenzoyl chromophore and the net transition electric moments, respectively. The dotted bands correspond to optically forbidden exciton bands for the polymer.

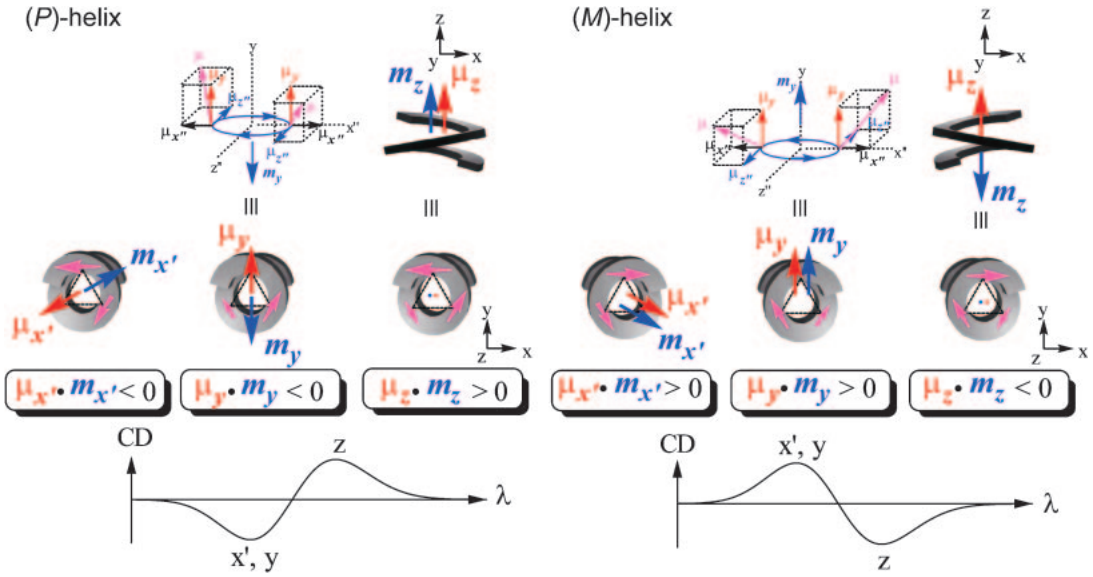

Figure 43. Overviews of the directions of the net electric ($\boldsymbol{\mu}$, red) and magnetic ($\boldsymbol{m}$, blue) transition dipole moments. The theoretically predicted CD signals are shown at the bottom. Note that the X'' and Z'' axes are tilted slightly compared with the x and z axes. The blue circle represents a circulation of charge arising from the coupling of two transition electric moments.

block copolymer **81** (solid line) was more complex than that of poly(isocyanide) without a porphyrin side chain **82** (dotted line), since a broad CD due to poly(isocyanide) **82** is superimposed on the exciton-type sharp CD signal due to the porphyrin moiety. However, after subtraction of the CD signal of the poly(isocyanide) **82** from the CD signal of the block copolymer **81**, a plus-to-minus pattern appeared in ascending energy, so that the helix sense of this poly(isocyanide) was experimentally determined to be right-handed, which was exactly opposite the proposal from calculations.[78]

9. Circular Dichroism of Cyclodextrin–Chromophore Systems

Many physical chemists are interested in examining the polarization direction or assignments of the absorption bands of chromophoric molecules. We wanted to demonstrate the utility of CD spectroscopy in this direction in the cyclodextrin (CDx)–chromophore system, which can be realized by simply mixing a chromophore and CDxs in water. Since water is used as the solvent, we can collect CD spectra at as short a wavelength as ca. 190 nm, which is a big advantage, particularly for small molecules having absorption at shorter wavelength. Since it has been established using CD spectroscopy for CDx–chromophore 1:1 complexes that transitions parallel to the axis of CDxs produce positive CD sign while those normal to it show negative CD sign,[76] we can determine the polarization direction of the chromophore trapped in their cavity. Conversely, using chromophoric molecules whose polarization of the band is known, the inclusion type can be conjectured. At the end of this section, the acceleration of charge-transfer (CT) complex formation in the presence of CDx is also reported.

Of the many compounds examined, the following are the most interesting cases. A) 2,2′- and 4,4′-bipyridyl:[79] In this case, the one and only inclusion type is a so-called "axial inclusion," in which the long axis of the molecule parallels the axis of CDxs. As can be seen in Figures 45a and 45b, the CD envelope at the longest wavelength is positive and negative for 2,2′- and 4,4′-bipyridyl, respectively; however, that of the second band is positive for both compounds. Although this was previously predicted by MCD study,[80] it was confirmed experimentally by CD spectroscopy for the first time. B) Biphenyls di-substituted at para positions either by electron-withdrawing or electron-donating groups:[79] In this case also (Figures 45c and 45d), the only conceivable inclusion type is axial inclusion. With respect to the longest absorption bands, a minus-to-plus CD signal was observed in ascending energy for all molecules, indicating that two transitions are included in one envelope of the electronic absorption spectra. With respect to biphenyls containing electron-withdrawing groups, the result was opposite in sign from that anticipated at that time from calculations.[81] C) *p*-Dimethylaminobenzoic acid:[82] When CD spectra were recorded for this compound and its anionic compound (i.e., at neutral pH and alkaline pH (Figures 45e and 45f), the CD sign of the band at the second longest wavelength changed from plus to minus, indicating that the polarization for the acid form is along the long axis while that of the anionic form is along the short axis. Thus, the polarization direction of this band varies, depending on whether the carboxyl group is dissociated or not. D) Pyrenetetrasulfonate:[83] The polarization direction of the absorption bands of pyrene had been well established as short as ca. 240 nm[84] and by us up to ca. 200 nm using the β-CDx–pyrene system (Figure 45g).[79] Using this information and considering its molecular size, the symmetrically substituted 1,3,6,8-pyrenetetrasulfonate appeared to be the best molecule to realize a so called "lid type inclusion." If this is the case, the CD signals should all be negative corresponding to the short- and long-axis polarized transitions, since both these axes of pyrene become perpendicular to the axis of CDx. This was indeed confirmed (Figure 45h). E) Ferrocene:[85] From its molecular size, ferrocene and β-CDx can only make an "axial inclusion." In the d–d band region of ferrocene (ca. 350–550 nm), the CD signal was plus in sign.

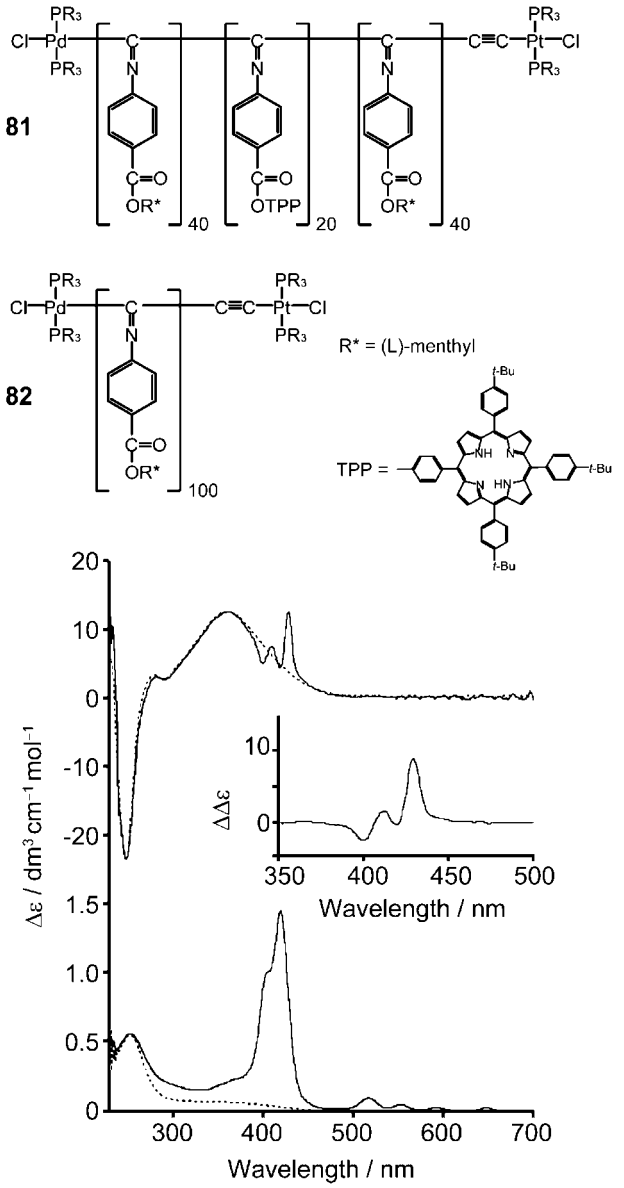

Figure 44. Structures of optically active poly(aryl isocyanide) containing L-menthyl pendant **82** (dotted lines) and that containing both L-menthyl and porphyrin pendant groups **81** (solid lines), and their electronic absorption and CD spectra.

Using this information and also a ferrocene derivative whose two cyclopentadienyl rings were linked by a crown ether unit, it was found that γ-CDx can form an equatorial inclusion with ferrocene, where in the above d–d band region, CD was minus in sign (Figure 45i). F) Pyrene–γ-CDx:[86] The band of pyrene at the longest wavelength is polarized along the long axis (Figure 45g).[84] Associated with this band, pyrene in γ-CDx (2:1 complex, confirmed by Job's continuous variation experiments) shows a minus-to-plus CD pattern in ascending energy, so that it was confirmed that two pyrene molecules take the form of a left-handed conformer in the cavity of γ-CD (Figure 45j). G) Charge-transfer complex formation in CDxs:[87] If we dissolve electron-deficient and -rich compounds in solution, they may form CT complexes. Therefore, various electron-deficient and -rich compounds were tested for this purpose in the presence of either β- or γ-CDx in water. Although γ-CDx had been known to accommodate two identical aromatic molecules such as naphthalene, anthracene,[88] or pyrene,[86] it was found that not only γ-CDx but even β-CDx can also trap two different aromatic molecules in their cavity. This was confirmed using particularly α-naphthylacetate and picric acid as an electron-donor and -acceptor, respectively.

10. Concluding Remarks

Large aromatic molecules such as porphyrins and phthalocyanines are convenient molecules for theoretical study, due to 1) their symmetry and size, 2) their ease of substitution, 3) their varied central metals, and 4) the fact that their planarity can be systematically changed, in addition to relatively easy oligomerization. Thus, for these reasons, many researchers are engaged in studying these compounds. A problem however, is that not many people are familiar with both synthesis and theory, so that good systems for theoretical study are not always presented. One of our aims was to present exemplary systems for understanding the physical properties of these compounds through the use of various spectroscopy. In particular, we were able to show the usefulness of MCD spectroscopy in elucidating the electronic structures of aromatic molecules, and the beauty and powerfulness of CD spectroscopy in clarifying the three-dimensional conformations of natural and artificial molecules.

In some cases, the experimental data could be explained only by concept, and in other cases the results were interpreted with the help of MO calculations. In the field of porphyrins and phthalocyanines, it is becoming harder to show new systems which are intriguing from the standpoint of electrochemistry and spectroscopy, since work on easy systems has become almost exhausted. We hope at least workers will use these spectroscopic and electrochemical techniques properly, since the equipment can be found in most of the universities and institutes in Japan. As shown in some of our studies, nature reveals the beauty of compounds through careful, intensive, and proper analysis of their spectral and electrochemical data. The selection or preparation of proper systems is, of course, prerequisite.

It is impossible for one group to do everything, and for us, the polymer systems were provided by experts of polymer synthesis. Interplay of the workers in different fields is necessary in deepening the understanding of complex systems. Although some researchers, particularly in the rural universities, suffer from an insufficient research budget, I would like to ask our government to supply at least the minimum amount of research budget to carry out research to these people in order to foster specialists in various fields, since discussion among the specialists can open new areas of chemistry.

The work from my laboratory has been the result of hard work by many people. I hereby acknowledge people who stayed in my laboratory. This work was partly supported by a Grant-in-Aid for Scientific Research on Innovative Areas (No. 20108001, "pi-Space") from the Ministry of Education, Culture, Sports, Science and Technology, Japan.

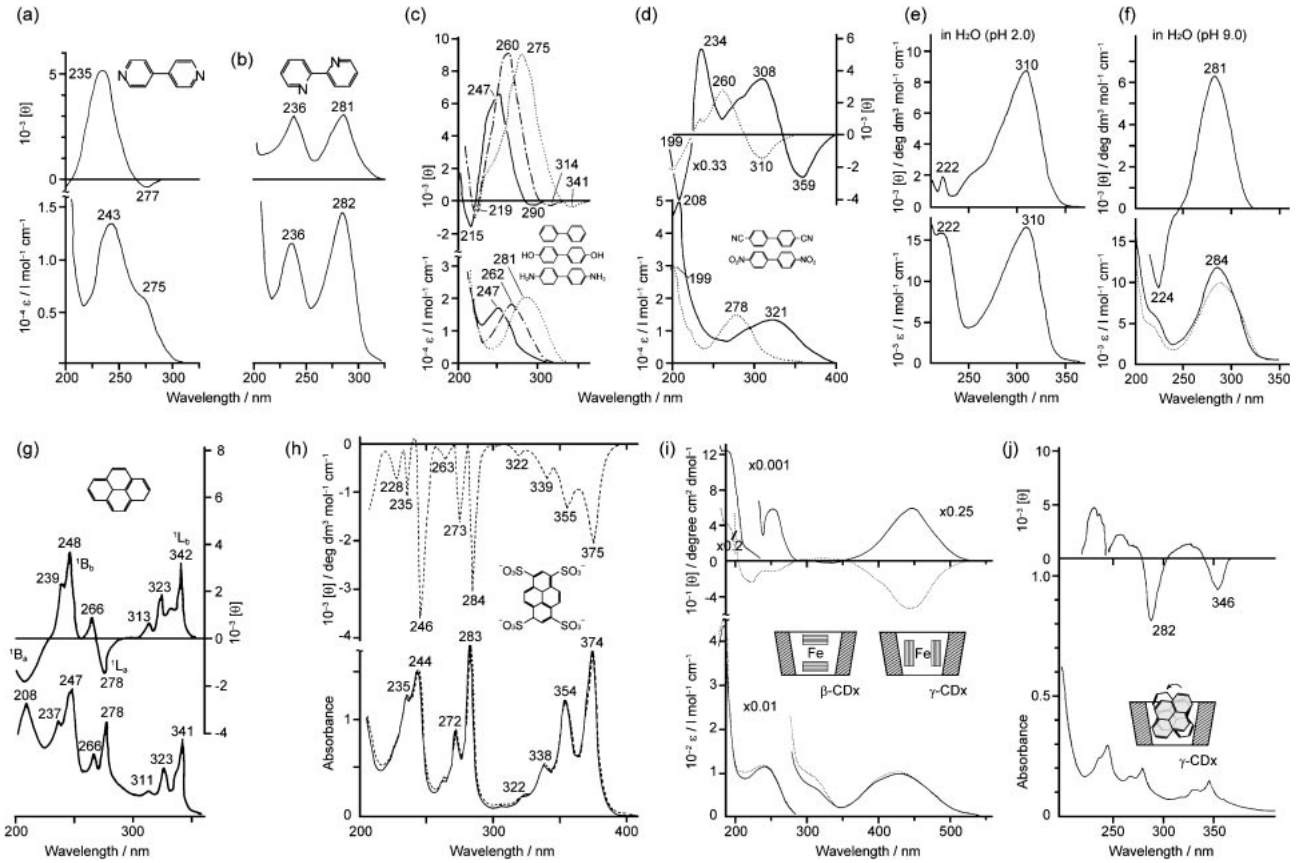

Figure 45. Electronic absorption and CD spectra of aromatic molecules trapped in the cavity of cyclodextrin. (a) 4,4′-bipyridyl, (b) 2,2′-bipyridyl, (c) biphenyl (solid lines), 4,4′-dihydroxybiphenyl (dotted broken lines), and 4,4′-diaminobiphenyl (dotted lines), (d) 4,4′-dicyanobiphenyl (broken lines) and 4,4′-dinitrobiphenyl (solid lines), (e) *p*-dimethylaminobenzoic acid at pH 2, (f) *p*-dimethylaminobenzoic acid at pH 9, (g) pyrene, (h) 1,3,6,8-pyrenetetrasulfonate (pH 9), (i) ferrocene in the presence of either β-CDx (solid lines) or γ-CDx (dotted lines), and (j) pyrene. (a)–(g) were taken in the presence of β-CDx while (h) and (j) were recorded in the presence of γ-CDx.

References

1 N. Kobayashi, *Bull. Chem. Soc. Jpn.* **2002**, *75*, 1.

2 A. Meller, A. Ossko, *Monatsh. Chem.* **1972**, *103*, 150.

3 H. Kietaibl, *Monatsh. Chem.* **1974**, *105*, 405.

4 N. Kobayashi, R. Kondo, S. Nakajima, T. Osa, *J. Am. Chem. Soc.* **1990**, *112*, 9640; N. Kobayashi, T. Ishizaki, K. Ishii, H. Konami, *J. Am. Chem. Soc.* **1999**, *121*, 9096.

5 N. Kobayashi, *J. Chem. Soc., Chem. Commun.* **1991**, 1203.

6 T. Fukuda, J. R. Stork, R. J. Potucek, M. M. Olmstead, B. C. Noll, N. Kobayashi, W. S. Durfee, *Angew. Chem., Int. Ed.* **2002**, *41*, 2565.

7 T. Fukuda, M. M. Olmstead, W. S. Durfee, N. Kobayashi, *Chem. Commun.* **2003**, 1256.

8 M. S. Rodríguez-Morgade, S. Esperanza, T. Torres, J. Barberá, *Chem.—Eur. J.* **2005**, *11*, 354.

9 J. R. Stork, J. J. Brewer, T. Fukuda, J. P. Fitzgerald, G. T. Yee, A. Y. Nazarenko, N. Kobayashi, W. S. Durfee, *Inorg. Chem.* **2006**, *45*, 6148.

10 N. Kobayashi, *J. Porphyrins Phthalocyanines* **1999**, *3*, 453.

11 Y. Inokuma, J. H. Kwon, T. K. Ahn, M.-C. Yoon, D. Kim, A. Osuka, *Angew. Chem., Int. Ed.* **2006**, *45*, 961.

12 N. Kobayashi, Y. Takeuchi, A. Matsuda, *Angew. Chem., Int. Ed.* **2007**, *46*, 758.

13 Y. Takeuchi, A. Matsuda, N. Kobayashi, *J. Am. Chem. Soc.* **2007**, *129*, 8271.

14 M. Gouterman, in *The Porphyrins, Vol. III: Physical Chemistry, Part A*, ed. by D. Dolphin, Academic Press, New York, **1978**.

15 K. M. Kadish, E. Caemelbecke, G. Royal, in *the Porphyrin Handbook*, ed. by K. M. Kadish, R. Guilard, K. M. Smith, Academic Press, New York, **2000**, Vol. 8, Chap. 55; J. H. Furhop, K. M. Kadish, D. G. Davis, *J. Am. Chem. Soc.* **1973**, *95*, 5140.

16 a) N. Kobayashi, H. Miwa, V. N. Nemykin, *J. Am. Chem. Soc.* **2002**, *124*, 8007. b) N. Kobayashi, S. Nakajima, H. Ogata, T. Fukuda, *Chem.—Eur. J.* **2004**, *10*, 6294.

17 N. Kobayashi, H. Konami, in *Phthalocyanines: Properties and Applications*, ed. by C. C. Leznoff, A. B. P. Lever, VCH, New York, **1996**, Vol. IV, Chap. 9.

18 J. Michl, *J. Am. Chem. Soc.* **1978**, *100*, 6801; J. Michl, *J. Am. Chem. Soc.* **1978**, *100*, 6812.

19 J. Mack, M. J. Stillman, N. Kobayashi, *Coord. Chem. Rev.* **2007**, *251*, 429.

20 J. Mack, Y. Asano, N. Kobayashi, M. J. Stillman, *J. Am. Chem. Soc.* **2005**, *127*, 17697.

21 N. Kobayashi, T. Fukuda, *J. Am. Chem. Soc.* **2002**, *124*, 8021.

22 O. Matsushita, A. Muranaka, Y. Kobayashi, N. Kobayashi, *Heterocycles* **2007**, *74*, 321.

23 N. Kobayashi, *Chem. Commun.* **1998**, 487.

24 N. Kobayashi, J. Mack, K. Ishii, M. J. Stillman, *Inorg. Chem.* **2002**, *41*, 5350.
25 T. R. Janson, A. R. Kane, J. F. Sullivan, K. Knox, M. E. Kenney, *J. Am. Chem. Soc.* **1969**, *91*, 5210.
26 T. Koyama, T. Suzuki, K. Hanabusa, H. Shirai, N. Kobayashi, *Inorg. Chim. Acta* **1994**, *218*, 41.
27 H. Miwa, K. Ishii, N. Kobayashi, *Chem.—Eur. J.* **2004**, *10*, 4422.
28 N. Kobayashi, E. A. Luk'yanets, *Fine Chemicals* **1997**, *26*, 5.
29 K. Ishii, A. Takayanagi, S. Shimizu, H. Abe, K. Sogawa, N. Kobayashi, *Free Radical. Biol. Med.* **2005**, *38*, 920.
30 K. Ishii, M. Shiine, Y. Shimizu, S. Hoshino, H. Abe, K. Sogawa, N. Kobayashi, *J. Phys. Chem. B* **2008**, *112*, 3138.
31 K. Ishii, H. Itoya, H. Miwa, M. Fujitsuka, O. Ito, N. Kobayashi, *J. Phys. Chem. A* **2005**, *109*, 5781.
32 K. Ishii, H. Itoya, H. Miwa, N. Kobayashi, *Chem. Commun.* **2005**, 4586.
33 T. Fukuda, N. Kobayashi, *Chem. Lett.* **2002**, 866.
34 G. E. Ficken, R. P. Linstead, E. Stephen, M. Whalley, *J. Chem. Soc.* **1958**, 3879.
35 E. A. Makarova, G. V. Korolyova, O. L. Tok, E. A. Luk'yanets, *J. Porphyrins Phthalocyanines* **2000**, *4*, 525.
36 H. Miwa, E. A. Makarova, K. Ishii, E. A. Luk'yanets, N. Kobayashi, *Chem.—Eur. J.* **2002**, *8*, 1082.
37 J. F. Kleibeuker, R. J. Platenkamp, T. J. Schaafsma, *Chem. Phys.* **1978**, *27*, 51.
38 T. Fukuda, E. A. Makarova, E. A. Luk'yanets, N. Kobayashi, *Chem.—Eur. J.* **2004**, *10*, 117.
39 N. Kobayashi, T. Fukuda, *Chem. Lett.* **2004**, *33*, 32.
40 E. A. Makarova, T. Fukuda, E. A. Luk'yanets, N. Kobayashi, *Chem.—Eur. J.* **2005**, *11*, 1235.
41 T. Fukuda, S. Masuda, N. Kobayashi, *J. Am. Chem. Soc.* **2007**, *129*, 5472.
42 T. Fukuda, S. Masuda, N. Hashimoto, N. Kobayashi, *Inorg. Chem.* **2008**, *47*, 2576.
43 a) M. O. Senge, in *the Porphyrin Handbook*, ed. by K. M. Kadish, R. Guilard, K. M. Smith, Academic Press, New York, **1999**, Vol. 1, Chap. 66. b) A. B. P. Lever, *Adv. Inorg. Chem.* **1965**, *7*, 27.
44 T. Fukuda, S. Homma, N. Kobayashi, *Chem.—Eur. J.* **2005**, *11*, 5205.
45 N. Kobayashi, T. Fukuda, K. Ueno, H. Ogino, *J. Am. Chem. Soc.* **2001**, *123*, 10740.
46 T. Fukuda, T. Ishiguro, N. Kobayashi, *Tetrahedron Lett.* **2005**, *46*, 2907.
47 T. Fukuda, S. Homma, N. Kobayashi, *Chem. Commun.* **2003**, 1574.
48 T. Fukuda, K. Ono, S. Homma, N. Kobayashi, *Chem. Lett.* **2003**, *32*, 736.
49 a) P. M. Burnham, M. J. Cook, L. A. Gerrard, M. J. Heeney, D. L. Hughes, *Chem. Commun.* **2003**, 2064. b) C. C. Leznoff, L. S. Black, A. Hiebert, P. W. Causey, D. Christendat, A. B. P. Lever, *Inorg. Chim. Acta* **2006**, *359*, 2690.
50 M. J. Cook, J. McMurdo, A. K. Powell, *J. Chem. Soc., Chem. Commun.* **1993**, 903; I. Chambrier, M. J. Cook, M. Helliwell, A. K. Powell, *J. Chem. Soc., Chem. Commun.* **1992**, 444; M. Helliwell, A. Deacon, K. J. Moon, A. K. Powell, M. J. Cook, *Acta Crystallogr., Sect. B* **1997**, *53*, 231.
51 N. Kobayashi, *Coord. Chem. Rev.* **2001**, *219–221*, 99.
52 J.-C. Marchon, R. Ramasseul, in *the Porphyrin Handbook*, ed. by K. M. Kadish, R. Guilard, K. M. Smith, Academic Press, New York, **2003**, Vol. 11, Chap. 64.
53 N. Kobayashi, R. Higashi, B. C. Titeca, F. Lamote, A. Ceulemans, *J. Am. Chem. Soc.* **1999**, *121*, 12018.
54 A. Muranaka, M. Okuda, N. Kobayashi, K. Somers, A. Ceulemans, *J. Am. Chem. Soc.* **2004**, *126*, 4596.
55 M. Namikoshi, H. Nakata, H. Yamada, M. Nagai, T. Saitoh, *Chem. Pharm. Bull.* **1987**, *35*, 2761.
56 These four equations can be applied to any two chromophore systems, and are shown in a text book of CD.[76]
57 A. Muranaka, K. Yoshida, T. Shoji, N. Moriichi, S. Masumoto, T. Kanda, Y. Ohtake, N. Kobayashi, *Org. Lett.* **2006**, *8*, 2447.
58 V. V. Borovkov, I. Fujii, A. Muranaka, G. A. Hembury, T. Tanaka, A. Ceulemans, N. Kobayashi, Y. Inoue, *Angew. Chem., Int. Ed.* **2004**, *43*, 5481.
59 N. Harada, K. Nakanishi, *Circular Dichroism Spectroscopy, Exciton Coupling in Organic Stereochemistry*, University Science Books, Mill Valley, CA, **1983**.
60 N. Kobayashi, U. Akiba, K. Takatori, A. Ueno, T. Osa, *Heterocycles* **1982**, *19*, 2011.
61 a) A. Muranaka, Y. Asano, A. Tsuda, A. Osuka, N. Kobayashi, *ChemPhysChem* **2006**, *7*, 1235. b) A. Tsuda, H. Furuta, A. Osuka, *J. Am. Chem. Soc.* **2001**, *123*, 10304.
62 a) N. Ishikawa, *J. Porphyrins Phthalocyanines* **2001**, *5*, 87, and some references therein. b) T. Miyahara, H. Nakatsuji, J. Hasegawa, A. Osuka, N. Aratani, A. Tsuda, *J. Chem. Phys.* **2002**, *117*, 11196.
63 N. Kobayashi, K. Nakai, *Chem. Commun.* **2007**, 4077.
64 A. Muranaka, M. Yokoyama, Y. Matsumoto, M. Uchiyama, A. Tsuda, A. Osuka, N. Kobayashi, *ChemPhysChem* **2005**, *6*, 171.
65 N. Kobayashi, *Coord. Chem. Rev.* **2002**, *227*, 129.
66 J. Jiang, Y. Bian, F. Furuya, W. Liu, M. T. M. Choi, N. Kobayashi, H.-W. Li, Q. Yang, T. C. W. Mak, D. K. P. Ng, *Chem.—Eur. J.* **2001**, *7*, 5059.
67 A. Muranaka, Y. Matsumoto, M. Uchiyama, J. Jiang, Y. Bian, A. Ceulemans, N. Kobayashi, *Inorg. Chem.* **2005**, *44*, 3818.
68 M. S. Rodriguez-Morgade, G. D. L. Torre, T. Torres, in *the Porphyrin Handbook*, ed. by K. M. Kadish, K. M. Smith, R. Guilard, Academic Press, New York, **2003**, Vol. 15, Chap. 99.
69 N. Kobayashi, S. Inagaki, V. N. Nemykin, T. Nonomura, *Angew. Chem., Int. Ed. Engl.* **2001**, *40*, 2710.
70 Using scanning tunneling microscopy, three cobalt atoms of the cobalt complex were found to be in a trianglar position (our unpublished data).
71 N. Kobayashi, A. B. P. Lever, *J. Am. Chem. Soc.* **1987**, *109*, 7433.
72 a) S. Yoshimoto, K. Suto, K. Itaya, N. Kobayashi, *Chem. Commun.* **2003**, 2174. b) S. Yoshimoto, K. Suto, A. Tada, N. Kobayashi, K. Itaya, *J. Am. Chem. Soc.* **2004**, *126*, 8020.
73 E. Charney, *The Molecular Basis of Optical Activity*, John-Wiley, New York, **1979**, Chap. 8.
74 A. Tanatani, A. Yokoyama, I. Azumaya, Y. Takakura, C. Mitsui, M. Shiro, M. Uchiyama, A. Muranaka, N. Kobayashi, T. Yokoyama, *J. Am. Chem. Soc.* **2005**, *127*, 8553.
75 H. Shimizu, A. Kaito, M. Hatano, *Bull. Chem. Soc. Jpn.* **1979**, *52*, 2678; H. Shimizu, A. Kaito, M. Hatano, *Bull. Chem. Soc. Jpn.* **1981**, *54*, 513; H. Shimizu, A. Kaito, M. Hatano, *J. Am. Chem. Soc.* **1982**, *104*, 7059; N. Kobayashi, T. Osa, *Bull. Chem. Soc. Jpn.* **1991**, *64*, 1878.
76 A. Rodger, B. Norden, *Circular Dichroism and Linear Dichroism*, Oxford University Press, Oxford, **1997**.
77 F. Takei, H. Hayashi, K. Onitsuka, N. Kobayashi, S.

Takahashi, *Angew. Chem., Int. Ed. Engl.* **2001**, *40*, 4092.
78 D. B. Amabilino, E. Ramos, J.-L. Serrano, T. Sierra, J. Veciana, *J. Am. Chem. Soc.* **1998**, *120*, 9126.
79 N. Kobayashi, S. Minato, T. Osa, *Makromol. Chem.* **1983**, *184*, 2123.
80 H. Uchimura, Doctral Thesis, Tohoku University, Sendai, **1980**.
81 H. Uchimura, A. Tajiri, M. Hatano, *Bull. Chem. Soc. Jpn.* **1981**, *54*, 3279.
82 a) N. Kobayashi, T. Osa, *Carbohydr. Res.* **1989**, *192*, 147. b) N. Kobayashi, *J. Chem. Soc., Chem. Commun.* **1989**, 1126.
83 N. Kobayashi, *J. Chem. Soc., Chem. Commun.* **1988**, 918.
84 F. D. Saeva, P. E. Sharpe, G. R. Olin, *J. Am. Chem. Soc.* **1973**, *95*, 7656.
85 N. Kobayashi, M. Opallo, *J. Chem. Soc., Chem. Commun.* **1990**, 477.
86 a) N. Kobayashi, R. Saito, Y. Hino, A. Ueno, T. Osa, *J. Chem. Soc., Chem. Commun.* **1982**, 706. b) N. Kobayashi, R. Saito, H. Hino, Y. Hino, A. Ueno, T. Osa, *J. Chem. Soc., Perkin Trans. 2* **1983**, 1031.
87 a) N. Kobayashi, A. Ueno, T. Osa, *J. Chem. Soc., Chem. Commun.* **1981**, 340. b) N. Kobayashi, R. Saito, A. Ueno, T. Osa, *Makromol. Chem.* **1983**, *184*, 837.
88 a) N. Kobayashi, Y. Hino, A. Ueno, T. Osa, *Bull. Chem. Soc. Jpn.* **1983**, *56*, 1849. b) M. Opallo, N. Kobayashi, T. Osa, *J. Inclusion Phenom.* **1989**, *7*, 413.

Nagao Kobayashi was born in January, 1950 in Nagano, Japan, the host city of the 1998 Winter Olympics. In 1978, he earned a Dr. of Science degree from Tohoku University based on a study of the magnetic circular dichroism spectroscopy of peroxidase and catalase. He later obtained a Dr. of Pharmacy degree, in 1986, based on a study of the electrocatalytic reduction of oxygen by water-soluble porphyrins and phthalocyanines. He was appointed as a research associate at the Chemical Research Institute of Non-Aqueous Solutions, and subsequently at the Pharmaceutical Institute, of Tohoku University, in 1983 and 1985, respectively. During this period, he also held visiting professor positions in the laboratories of Prof. A. B. P. Lever in Toronto, Canada from 1986–1987 and Prof. J. Simon at ESPCI, Paris (the institute where Pierre and Marie Curie discovered radium) in 1994. In 1995, he was appointed as a full professor of the Department of Chemistry in the Graduate School of Science at Tohoku University. His research interests cover many different areas of phthalocyanine and porphyrin chemistry with a strong focus on synthesis, electrochemistry, and optical spectroscopy. The MCD and CD spectroscopy of porphyrinoids is a key area of expertise. He currently has more than 300 publications (including original research articles, reviews, and book chapters).

Takamitsu Fukuda was born in Kushiro, Japan in 1976 and was educated at Tohoku University in Japan and at Umeå University in Sweden. He obtained a Ph.D. in Chemistry in 2004 in Professor Nagao Kobayashi's laboratory. From 2001–2002, he received a Research Fellowship for Young Scientists from the Japan Society for the Promotion of Science (JSPS). He was appointed as an assistant professor in the functional molecular chemistry group at Tohoku University, in 2002 and has been a lecturer since 2009. His research interests include the synthesis of phthalocyanine-based functional molecules, and their spectroscopic and electrochemical properties.